

1 Rift and plume: a discussion on active and passive rifting 2 mechanisms in the Afro-Arabian rift based on synthesis of 3 geophysical data

4 Ran Issachar^{1,2}, Peter Haas^{1,3}, Nico Augustin³ and Jörg Ebbing¹

5 ¹Institute for Geosciences, Kiel University, Geophysics, Kiel, Deutschland, ²Geological Survey of Israel, Jerusalem, Israel,

6 ³GEOMAR Helmholtz Centre for Ocean Research, Kiel, Deutschland

7 *Correspondence to:* Ran Issachar (ranis@gsi.gov.il)

8 Abstract

9 The causal relationship between the activity of mantle plumes and continental break-up is still elusive. The
10 Afro-Arabian rift system offers an opportunity to examine these relationships, in which an ongoing
11 continental break-up intersects a large Cenozoic plume-related flood basalt series. In the Afar region, the
12 Gulf of Aden, the Red Sea, and the Main Ethiopian Rift form an R-R-R triple junction within plume related
13 flood basalts series. We provide an up-to-date synthesis of the available geophysical and geological data
14 from this region. We map the rift architecture in the intersection region ~~by applying the using~~ Difference
15 in Gaussians ~~to the topography and the bathymetry~~ and ~~interpreting interpretation of~~ vertical gravity
16 gradients and Bouguer anomalies. With the aid of these methods we review the spatio-temporal
17 constraints in the evolution of the different features of the plume-rift system.

18 Our results show rough and irregular ~~morphologies morphology~~ of the Gulf of Aden and the Red Sea arms
19 in contrast to the symmetric, continuous, and smooth Main Ethiopian Rift. The triple junction formed by
20 the northeastward propagation of the Main Ethiopian rift ~~develops and developed~~ simultaneously to the
21 abandonment of the tectonic connection between the Red Sea and the Gulf of Aden through Bab al-
22 Mandab Strait. The onset of the triple junction was the last feature to develop in the plume-rift system
23 and marked a tectonic reorganization. By this time, all rift arms were sufficiently evolved and the break-
24 up between Africa and Arabia was already accomplished.

25 We argue that the classical active and passive rifting mechanisms cannot simply explain the progressive
26 development of the Afro-Arabian rift. Instead, we propose a plume-induced plate rotation, which includes
27 an interaction between active and passive mechanisms. In this tectonic scenario, the arrival of the Afar
28 plume provided a push force that promoted the rotation of Arabia around a nearby pole ~~located to the~~
29 northwest ~~to of~~ the plate boundary, enabling the rifting and, ultimately, the break-up of Arabia from Africa.

30

31 Short summary:

32 In this contribution, we explore the causal relationship between the arrival of the Afar plume and the
33 initiation of the Afro-Arabian rift. We mapped the rift architecture in the triple junction region using
34 geophysical data and reviewed the available geological data. We interpret a progressive development of
35 the plume-rift system and suggest an interaction between active and passive mechanisms in which the
36 plume provided a push-force that changed the kinematics of the associated plates.

37 1. Introduction

38 The causal dependency between the eruption of flood basalts and continental break-up is still unclear,
39 although a close occurrence between these two phenomena has been recognized for a long time.
40 Continental flood basalts, often referred to as traps, form large igneous provinces covering huge
41 continental areas (Bryan and Ferrari, 2013; Ernst, 2014). Continental flood basalts are often associated
42 with extensive volcanism during short time intervals, which are brought to the surface by deep-seated
43 mantle plumes (Richards et al., 1989; White and McKenzie, 1995; Koppers et al., 2021), although other
44 mechanisms were also suggested (e.g., Anderson, 1994, 2005). There is evidence for a close temporal and
45 spatial occurrence between the eruption of flood basalts and continental break-up. In particular, when
46 reconstructed back to their original plate tectonic configuration, a R-R-R triple junction is typically found
47 within the flood basalt areas (Morgan, 1971; Burke and Dewey, 1973; Buitert and Torsvik, 2014). Using the
48 geological record to examine the mutual dependency of these processes is challenging. It requires high-
49 precision in the temporal and spatial development of the volcanic and tectonic features, often obscured
50 by the overprint of different tectonic processes.

51 The Afar region in the central parts of the Afro-Arabian rift system is recognized as a key locality to examine
52 models of plume-rift association, offering a young and active case study in which a plume, regional uplift,
53 an R-R-R triple junction, break-up, and oceanic spreading co-exist and are superimposed (Fig. 1). Plume-
54 rift association is mainly explained as either ‘active’ (e.g., Sengör and Burke, 1978) or ‘passive’ (e.g., White
55 and McKenzie, 1989), with no interaction between those mechanisms. Despite the contrary implications,
56 the Afar case study was used as a prime example to support both the ‘active’ (e.g., Burke and Dewey, 1973)
57 and the ‘passive’ (e.g., White and McKenzie, 1989) mechanisms, and some authors argued that both
58 processes are required to explain the observations (e.g., Courtillot et al., 1999). The discrepancy can be
59 primarily attributed to the lack of accurate geological and geophysical evidence regarding the uplift,
60 volcanism and rifting phases. Moreover, ~~detailed compression between studies show that~~ changes in plate
61 motions and the activity of plumes ~~occurred concurrently~~, suggests new concepts in which plumes cause
62 rapid deviations in the kinematics of nearby plates (e.g., Cande and Stegman, 2011).

63 The purpose of this paper is to discuss the causal relationship between the Afar plume and rifting along
64 the Afro-Arabian rift system in light of the large amounts of data collected in recent years and the new
65 concepts derived from ~~studies of the Indian plate~~ ~~other case studies~~. For this, we first review the timing of
66 volcanism and uplifts in Ethiopia and Yemen, and, the timing of rifting along the Gulf of Aden, the Red Sea
67 and the Main Ethiopian rift. We further provide an analysis and interpretation of modern geophysical
68 datasets, including topography, bathymetry, ~~and~~ gravity, ~~and incorporated the distribution of offshore~~
69 magnetic anomalies, earthquakes ($M_L > 4$), and ~~onshore Quaternary volcanos-distribution~~. Using these
70 datasets, we map the architecture of the rifts and describe the development of rift segments. Finally, we
71 compare our results with recent models and other case studies in the world, aiming to shed light on the
72 causal relationship between mantle plumes and tectonic processes.

73

74 2. Active and passive mechanisms for plume-rift association

75 The existence of deep mantle convection and its interaction with the Earth’s lithosphere was already
76 pointed out by Wilson (1963), and a close occurrence to continental break-up was soon noticed by the

77 abundance of hotspots near many rift junctions (Morgan, 1971) and flood basalt volcanism along passive
78 margins (Richards et al., 1989). Although Morgan (1971) speculated that deep mantle convection has a
79 significant role in accelerating the overlying tectonic plates, it was later realized that slab-pull provides the
80 main driving force for plate motion (Forsyth and Uyeda, 1975). In their landmark paper, Burke and Dewey
81 (1973) presented 45 case studies of rift junctions associated with hot spots. They proposed a model in
82 which plume-associated uplift and volcanism precede and generate the rift arms, initiated from a triple
83 junction within the plume region. Afar was used as a first and prime example, highlighting its importance
84 as a young and active case study; however, they already noted a complex distribution of continental
85 fragments and magnetic anomalies (Burke and Dewey, 1973).

86 Following these insights, 'active' rifting models were developed to explain plume-rift associations (e.g.,
87 Keen, 1985; Moretti and Froidevaux, 1986; Campbell and Griffiths, 1990; Hill, 1991; White and McKenzie,
88 1995). These models generally propose that rifting can result from a combination of processes derived
89 from the actively rising head of an anomalously hot mantle. These mantle plumes impinge and erode the
90 base of the lithosphere, which prompt uplift and decompression melting, introduce internal extensional
91 forces and ultimately lead to break-up. Accordingly, regional uplift and volcanism are expected to precede
92 rifting, which would initiate from a triple junction above the mantle plume head (Fig. 2a).

93 Later contributions challenged the active view, arguing that a 'passive' asthenospheric upwelling can also
94 resolve the occurrence of flood basalt near rifts (firstly introduced by White and McKenzie, 1989). In this
95 view, rifting is initiated by the remote extensional stresses, usually along former sutures and weak zones,
96 regardless of underlying plumes. The production of massive volcanism is allowed when the thinned and
97 stretched lithosphere is underlain by a thermal anomaly in the mantle. The volcanism is generated by
98 decompression melting of the hot asthenospheric mantle, which passively rises. As plumes form large
99 areas of high temperatures in the mantle, massive volcanism is found on Earth's crust close to rifts.
100 Accordingly, subsidence is a precondition required for magmatism, and there is no triggering mechanisms
101 for a triple junction to form within the flood basalts region (Fig. 2b).

102 Although active and passive mechanisms have been discussed in the last 50 years, the role of plumes in
103 initiating rifting is still unclear and much debated. Even for well-studied and prime examples of plume-rift
104 association as the Siberian, Parana-Etendeka, Deccan, and Greenland traps, there is no agreement on
105 whether active processes initiated rifting (Geoffroy, 2005; Ivanov et al., 2015; Frizon De Lamotte et al.,
106 2015; Fromm et al., 2015; Mitra et al., 2017). Some authors emphasize the significance of pre-existing
107 lithosphere weaknesses along former sutures and structures (Buiter and Torsvik, 2014; Will and Frimmel,
108 2018), while others show the potential of plumes to thermally and chemically erode the base of the
109 lithosphere in the weakening process allowing rifting (Sobolev et al., 2011). Additionally, some models
110 demonstrate that mixed active-passive scenarios can better explain observation (Koptev et al., 2018), and
111 even that both mechanisms are needed to explain temporal variations in rifts (Huisman et al., 2001).

112 In addition to the dichotomic views, a complex relationship in which plumes can influence the horizontal
113 velocities of plates is suggested based on detailed plate reconstructions and numerical modeling (van
114 Hinsbergen et al., 2011, 2021; Cande and Stegman, 2011; Chatterjee et al., 2013; Pusok and Stegman,
115 2020). In these studies, an abrupt change in plate velocities is correlated to the arrival of a nearby plume
116 head. In the kinematic record of the Indian plate, the arrival of the Marion and Reunion plumes (associated
117 with the Morondava and Deccan LIPs) is synchronized with an abrupt plate speed-up and an Euler pole
118 shifting. During the arrival of the Reunion plume (at ~65 Ma), the acceleration of the Indian plate was
119 coupled with transitory slowing of the African plate (Cande and Stegman, 2011). Plume push forces,

120 sourced by the drag of the flowing asthenosphere, ~~were~~ shown as capable to change the ~~plate~~
121 kinematics of nearby plates and even trigger the formation of new plate boundaries by a mechanism
122 termed as plume-induced plate rotation (van Hinsbergen et al., 2021) (Fig. 2c).

123 3. Geological setting

124 The Afro-Arabian rift system extends from Turkey to Mozambique (McConnell and Baker, 1970) and is the
125 current episode of the Phanerozoic break-up of the East African continental plate (Bosworth, 2015). It
126 contains rifting in the Gulf of Aden, in the Red Sea, and in East Africa. In the center of that system, the
127 Ethiopian northwestern and southeastern plateaus represent an elevated topography with a highest peak
128 of 4,620 m (Ras Dashan) and an average elevation of 2000 m above sea level. This area is part of the so-
129 called African Superswell, a wide region of anomalously high topography comprising East Africa (Lithgow-
130 Bertelloni and Silver, 1998; Corti, 2009). In western Yemen, the Sarawat Mountains are the highest peaks
131 in the Arabian Peninsula, reaching more than 3,000 m, ~~at~~ only 100 km distance away from the shoreline
132 of the Red Sea. These mountains show a typical stair morphology with steep slopes at the western and
133 southern sides, while the eastern shows gentler downward slopes.

134 The Gulf of Aden is the most developed rift segment in the Afro-Arabian rift, with a mature and fully
135 developed oceanic spreading center connected to the mid-ocean ridge in the Indian Ocean. Six pairs of
136 magnetic anomalies associated with seafloor spreading are recognized along the Gulf of Aden (Fournier et
137 al., 2010) (Fig. 3). Oblique rifting and high-angle structural inheritance along the Gulf of Aden resulted in
138 multiple ridge segments and fracture zones (i.e., transform faults; Leroy et al., 2013; Autin et al., 2013;
139 Bellahsen et al., 2013; Duclaux et al., 2020).

140 At the northern parts, the rifting in the Red Sea is connected by the Dead Sea Fault to the Eurasian collision
141 zone along the Taurus-Zagros Mountains. The Red Sea is experiencing the last stages of break-up and early
142 stages of oceanic accretion. An oceanic spreading center with three pairs of ridge parallel magnetic
143 anomalies are recognized in the southern parts of the Red Sea (Schettino et al., 2016) (Fig. 3). ~~H~~ However,
144 oceanic crust is probably flooring most of the basin (Augustin et al., 2021).

145 The Main Ethiopian Rift is the northernmost section of the intra-continental rifting in East Africa, splitting
146 the not-yet well-individualized Somali plate from Africa (Chorowicz, 2005). ~~Current-Active~~ rifting in the
147 Main Ethiopian Rift is characterized by a narrow rift valley, in which volcanic and tectonic activities are
148 localized and influenced by oblique rifting (Corti, 2009).

149 The above-mentioned three rift arms meet in the Afar triangle (Fig. 3). It is a low elevated area compared
150 to the high Ethiopian plateaus and thus commonly referred to as the Afar 'depression'. Nevertheless, this
151 term is misleading as the Afar triangle is included within the rifted area and is geologically elevated from
152 the deep bathymetry of the Gulf of Aden and the Red Sea basins. The Afar triangle is mainly floored by
153 Pliocene and younger volcanic rocks, where Miocene volcanic series are exposed along the western
154 margins and at the elevated Danakil block. It comprises many volcanoes and axial volcanic ranges (Fig. 2),
155 where the northeastern side is characterized by transverse volcanic fields and the southwestern side by
156 central volcanoes (Varet, 2018). Two symmetric magnetic anomalies have been recognized in the Tendaho
157 graben, similar to those observed along spreading centers in the Gulf of Aden (Bridges et al., 2012). These
158 could be associated either with young oceanization or with linear anomalies developed in transitional crust
159 (Ebinger et al., 2017). Structurally, several mega-scale accommodation zones are connecting the ~~different~~

160 rift segments and ~~the location of a main~~ triple junction ~~location are~~ recognized at 11.0°N, 41.6°E ~~at~~ along
161 the Tendaho-Goba'ad Discontinuity (e.g, Tesfaye et al., 2003) (Fig. 3).

162 4. Temporal constraints

163 4.1. Flood basalts and uplift

164 Vast efforts were made to study the chemistry and chronology of flood basalts in East Africa (see review
165 by Rooney, 2017). Two phases of extensive flood basalt volcanism are associated with plume-lithosphere
166 interaction (Fig. 4). The early phase is mainly confined to southern Ethiopia and northern Kenya. The timing
167 of this event is poorly constrained to 45-35 Ma (George et al., 1998). The second phase of flood basalt
168 eruptions was more voluminous, more widespread, and shorter-lived. Earliest basalts of this phase date
169 back to 34 Ma near the Tana Basin in Ethiopia (Prave et al., 2016) and 31 Ma in western Yemen (Peate et
170 al., 2005) (Fig. 4). The traps accumulated very rapidly, in less than 6 Ma (Coulié et al., 2003), and include
171 tholeiitic to alkaline compositions of asthenosphere mantle source (Mattash et al., 2013). Thick sequences
172 of up to 2 km are observed within a widespread region in Ethiopia and Kenya (Bellieni et al., 1981; Wescott
173 et al., 1999; McDougall and Brown, 2009). It is commonly accepted that these flood basalts are of a deep-
174 seated mantle plume origin (Koppers et al., 2021). However, the formation mechanism is debatable and
175 may involve multiple plume impingements within a broad upwelling zone connected to the African
176 superplume in the lower mantle (Meshesha and Shinjo, 2008) or a single plume-lithosphere interaction
177 (Rooney, 2017).

178 An elevated topography is associated with the eruption of the flood basalts in Ethiopia. The flood basalts
179 are almost exclusively positioned within the elevated regions of the Ethiopian and Somalian plateaus and
180 the Sarawat Mountains in southwest Yemen (Fig. 1). ~~The~~ ~~D~~dynamic topography component supports up
181 to 1 km of present-day elevation of the Ethiopian and Somalian plateaus, supporting the significant
182 contribution of mantle convection to the regional uplift (Gvirtzman et al., 2016). Although the uplift
183 chronology is not easily resolved, recent studies infer it is a long-term feature already ~~present~~ ~~active~~ before
184 the emplacement of the flood basalts (Sembroni et al., 2016; Faccenna et al., 2019). Regional uplift is
185 estimated to begin before 40 Ma, with maximal uplifts between 12 and 28 Ma, reaching an average
186 elevation of 2,500 m (Fig. 4) (Sembroni et al., 2016).

187 4.2. Gulf of Aden

188 The beginning of continental rifting in the Gulf of Aden relies on the dating of sedimentary sequences,
189 published in the 90's (see Bosworth et al., 2005 for a review). Onshore outcrops in Yemen (Watchorn et
190 al., 1998) and in Oman (Roger et al., 1989) and offshore wells (Hughes et al., 1991), suggest that rifting in
191 the central and eastern Gulf of Aden began at early to mid-Oligocene, within the Rupelian (33.9 - 27.8 Ma).
192 Syn-rift sediments from the central Yemeni margins indicate that rift flank uplift occurred before any
193 significant regional extension. The ~~continental rifting~~ climax ~~of continental rifting~~ is estimated between 20
194 and 18 Ma (Watchorn et al., 1998). Radiometric dating indicates that the margins became stable already
195 in the Early Miocene (Bosworth et al., 2005), and rift-to-drift transition is interpreted to occur between
196 ~21.1 and ~17.4 Ma (Watchorn et al., 1998). The seafloor spreading center in the Gulf of Aden is
197 ~~recognized~~ ~~developed~~ along most of its length and is connected to the mid-ocean ridge in the Indian Ocean
198 through the Sheba Ridge (Gillard et al., 2021). In the central Gulf of Aden, magnetic isochrons suggest

199 opening rates of ~27 mm/a prior to 11 Ma, and a slowdown after 11 Ma (Fig. 4). Chron 5C (purple stripes
200 in Fig. 3; 16.0 Ma) is present along the Gulf of Aden up to the Shukra al Sheik discontinuity (Fig. 3; Fournier
201 et al., 2010). This implies that the spreading center developed very rapidly, spreading over more than 700
202 km in less than 1.5 Ma. This fast propagation ceased at the Shukra al Sheik discontinuity. The youngest
203 magnetic isochrons (2A, 2.6 Ma) are recognized up to ~~longitude-43.9°E~~ in the eastern Gulf of Tadjoura,
204 ~150 km west to the Shukra al Sheik discontinuity, indicating that along this segment, the ridge propagated
205 westward at an average rate of ~11 mm/a, in the last 16 Ma. Within the Gulf of Tadjoura, no direct
206 evidence of oceanic spreading was reported ~~in the literature to our best knowledge.~~

207 4.3. Red Sea

208 Sedimentary sequences from offshore drillings suggest that rifting in the Red Sea postdated the rifting in
209 the Gulf of Aden by a few million years (Bosworth et al., 2005). Independent studies suggest that rifting
210 had begun simultaneously along the entire Red Sea at late Oligocene-Early Miocene, ~~at~~ ~23 Ma (Plaziat et
211 al., 1998; Szymanski et al., 2016; Stockli and Bosworth, 2018; Morag et al., 2019). Magnetic isochrons
212 associated with seafloor spreading are recognized at the southern parts of the Red Sea (Fig 3 ; Girdler and
213 Styles, 1974). However, oceanic lithosphere is probably abundant along most of the basin (Augustin et al.,
214 2021). Chron 3 (4.2 Ma) is only present between ~~latitudes-16°N~~ and 18°N, while chrons 2A (2.6 Ma) and 2
215 (1.8 Ma) are present up to ~~latitude-22°N~~ (Schettino et al., 2016). The recognition of Chron 5 (10 Ma) in the
216 central Red Sea was recently suggested to mark the beginning of seafloor spreading (Okwokwo et al.,
217 2022). Structural reconstructions, geodetic measurements, and magnetic anomalies suggest an opening
218 rate of ~11 mm/a up to ~4.6 Ma, an abrupt increase in ~~the~~ opening rate to ~25 mm/a between 4.6 and 1.8
219 Ma and a decrease to ~14 mm/a (Fig. 4 ; Schettino et al., 2018). The southern edges of the magnetic chrons
220 suggest that the southern Red Sea ridge propagated 50 km southwards, between 4.2 to 2.6 Ma (~30 mm/a).
221 Since 2.6 Ma, the Red Sea ridge has not propagated southward, probably due to the decrease in angular
222 velocity of Danakil relative to Arabia (Fig. 3 ; Schettino et al., 2018).

223 4.4. Main Ethiopian Rift

224 ~~The onset~~Age of faulting and volcanism along segments of the Main Ethiopian rift suggest a diachronous
225 development of the different segments of the Main Ethiopian Rift (e.g. Bonini et al., 2005). However, there
226 is no agreement regarding the exact timing of events and even the propagation trend of the rift.
227 Reconstructions based on magnetic anomalies from the Southwest Indian ridge suggest an upper limit for
228 the Nubia-Somalia separation at ~19 Ma, including large uncertainties regarding the rates and directions
229 of the relative motion pre-16 Ma (DeMets and Merkouriev, 2016) (Fig. 4). Geochronological data suggest
230 that volcanism and rifting in East Africa started at the Turkana depression in southern Ethiopia at 50 Ma
231 (Varet, 2018) and episodically propagated ~~northwards north,~~ However, it is still a matter of debate if
232 there is a general propagation pattern or if different segments propagated in different directions (see figs
233 42-44 in Corti, 2009). Nevertheless, radiometric dating of structural features indicates that extension
234 commenced at ~11 Ma within the northern Main Ethiopian Rift (Wolfenden et al., 2004).

235 In summary, regional uplift and flood basalt volcanism in Ethiopia preceded the rifting of the Afro-Arabian
236 rift (e.g., Rooney, 2017). The rift arms developed ~~diachronically at different times, with the onset of when~~
237 rifting in the eastern Gulf of Aden ~~occurring started~~ during the late phases of flood basalt volcanism (at
238 ~30 Ma) whereas rifting in the Red Sea (at ~23 Ma) and the Main Ethiopian Rift (at ~19 Ma) ~~started in a~~
239 ~~lag of lagged by~~ ~5-7 Ma ~~after flood basalt volcanism.~~

240 5. Data and Methods

241 We used bathymetry (Gebco compilation) and topography (SRTM 15+) data to identify morphotectonic
242 features. To highlight and map the architecture of the margins and axes of the rifts, we applied the
243 Difference of Gaussians (Fig. 5) method to the topography and the bathymetry grids (Akram et al., 2017).
244 This method allows a fast and accurate edge detection of elevation using active spatial bandpass filtering.
245 We applied luminance coloring to the resulting grid using the open-source image processing software
246 Gimp.org.

247 To study density-related shallow crustal structures, we used the satellite altimetry-derived vertical gravity
248 gradient (VGG) model of Sandwell et al. (2014), offering 1 arc-min resolution at offshore regions. As higher
249 frequencies are intensified in the spectral power of the VGG, its anomalies are more source-localized and
250 shallow-sensitive than free-air anomalies. To enhance the edges associated with the VGG, we applied a
251 linear 11-colors colormap, further applied transparency to the VGG map, and projected it on a shaded
252 relief (Fig. 6a).

253 To study deeper crustal structures and eliminate the topography effect, we used Bouguer gravity anomaly
254 (BGA), derived from the XGM2019 gravity model (Zingerle et al., 2020), calculated with a grid step of 0.1
255 degrees. The XGM2019 is the most updated global gravity model of the International Centre for Global
256 Earth Models (ICGEM) and is provided in terms of spherical harmonics up to 2159 degrees (Ince et al.,
257 2019; Zingerle et al., 2020). In addition, we applied a linear 240-colors colormap to enhance BGA
258 structures, further applied transparency to the BGA map, and projected it on a shaded relief (Fig. 6b).

259 To better correlate and discriminate crustal structures and rift features, we considered 1913 earthquake
260 locations (Fig. 3) from the International Seismological Centre catalog with minimum magnitudes ~~above~~
261 4 ML, recorded between 1964 and 2019. To better infer recent tectonic and volcanic activity, we further
262 considered the locations of Quaternary onshore volcanoes (Fig. 3), from the Global Volcanism Program
263 (Smithsonian Institution) and Google Earth mapping.

264 6. Results

265 6.1. Rift margins

266 The most prominent morphological feature of the rift system is the escarpment along its shoulders. The
267 escarpments mark the rift margin as they distinguish between (1) uplifted pre-rift rocks of the Arabo-
268 Nubian shield or trap basalts sequences and (2) Quaternary arid fluvial sediments or young volcanic
269 sequences, although several continental crustal fragments are present within the Afar Triangle. The edge
270 detection analysis of topography and bathymetry data allows us to outline the rift margins (Fig. 5). This
271 method highlights high frequency details, ~~where in Fig 5,~~ Steep gradients are shown in bright colors and
272 moderate gradients in grey colors (~~in Fig 5~~).

273 In the Red Sea, the escarpments are generally continuous with an average rift width of 440 ± 20 km
274 (calculated perpendicular to the Red Sea axis in the study area), and a general increase in rift width from
275 north to south (Fig. 5b). We identify two segments that mark an abrupt change in rift orientation and rift
276 width: (1) Below 15.5°N on the African margin and 18°N on the Arabian margin (segment I in Fig. 5), the
277 escarpment deviates from its general parallel to the Red Sea trend, bending towards the Afar region. The
278 escarpment is characterized by seismic activity from that point on the African side, which is also considered

279 the northern point of the western Afar margins (Zwaan et al., 2020a). (2) Below 12.5°N on the African
280 margin and 15°N on the Arabian margin (segment II in Fig. 5), we identify another abrupt change, both in
281 the orientation and the width of the rift. That point on the African margin is the intersection of the
282 Tendaho-Goba'ad Discontinuity with the Western Afar Margins (Tesfaye et al., 2003). We note that these
283 changes are noticeable and similar on the African and Arabian sides (Fig. 5a).

284 In the Gulf of Aden, the escarpments generally follow the trend of the basin (Fig 5). In the western parts,
285 the escarpments are ~~irregular/less straight~~ and less continuous than those of the Red Sea and generally
286 reflect the sinistral basin structures. This morphology is well explained by oblique rifting along the Gulf of
287 Aden (Leroy et al., 2013). The average rift width in the study area is 470 ± 45 km (calculated rift-
288 perpendicular), with a general eastward increase (565 km at 47.5°E and 420 km at 43.2°E; Fig. 5b). We
289 recognize an abrupt change in rift width along three lines (III-V in Fig. 5), which are associated with fracture
290 zones. Along the Somalian margin, prominent sinistral offsets are recognized along lines III and V. This
291 escarpment segment is a morphological continuation of the Tendaho-Goba'ad Discontinuity lineament,
292 and is also prominent in the VGG map (Fig. 6a).

293 Although recognizable in the processed topography map, the rift shoulders are ~~gentler/less sharp~~ in the
294 Main Ethiopian Rift (Fig. 5a). They are prominent in the gravity data as they are associated with VGG and
295 BGA highs (see profile A in Fig. 9). In the Afar region, the margins show a funnel shape (Fig. 5a). The distance
296 between the Somalian and Ethiopian escarpments is steadily and monotonically increasing from the Main
297 Ethiopian Rift to the Tendaho-Goba'ad Discontinuity (Fig. 5b), suggesting that this segment is intact and
298 non-disturbed by the other arms of the rift system.

299 In summary, the rift margins of the Red Sea and the Gulf of Aden are interrupted with ~~in~~ the proximity to
300 the Afar triangle, whereas the margins of the Main Ethiopian Rift smoothly funnel into the Afar triangle.

301 6.2. Rift axes

302 Along the Red Sea and the Gulf of Aden basins, the rift axes are distinctively characterized by deep and
303 sharp bathymetric troughs, VGG lows, BGA highs, and intense seismic activity (Fig. 3 ~~and Fig 6~~). However,
304 with the proximity to the Afar region, the rift axes change their characteristics.

305 The rift axis along the Red Sea is outlined by a deep and wide axial trough that ends at 14.5°N,
306 approximately 400 km from the triple junction (Fig. 7a). South of 14.5°N, we find geophysical evidence
307 that the rift axis is bent westwards, ~~running meeting the~~ onshore at the Bay of Beylul (white dashed line
308 in Fig. 7b). The VGG signature and the bathymetry display highs along the walls (50 Eotvos) and lows along
309 the center (Fig. 7b and profile B). A trail of volcanic islands follows this path (Hanish-Zukur Islands; Fig. 3),
310 and the alignments of volcanic cones and vents on the islands are orthogonal to the trail of the islands
311 (Mitchell and Bosworth, (in press); Gass et al., 1973). A general trend of recent magmatic bodies onshore
312 meets this line at the Bay of Beylul (Fig. 3). However, major fault sets are not observed in the onshore area
313 of Beylul (Rime et al., 2023). In addition, a best fit GPS-based rigid block model suggests a block boundary
314 along this path (Viltres et al., 2020), which is also supported by the fact that the rotation of Danakil relative
315 to Arabia stopped around $t \sim 0.3$ Ma (following Schettino et al., 2018 and personal communication). In
316 addition ~~to~~, the bent axial segment, a typical gravity signature of the Red Sea rift axis, with a 20 mGal
317 central BGA peak and 60 – 40 Eotvos VGG side peaks, is also recognized along the connection of the Red
318 Sea with the Gulf of Aden at Bab al Mandab Strait (13.2°N to 12.3°N; Fig. 7 profile CC'). Nevertheless, no
319 earthquakes, volcanic activity or faulted ~~bathymetry morphology~~ is ~~found~~ ~~observed~~ along this segment,

320 thus we propose that this segment is not an active rift axis. However, diluted activity is inferred from the
321 low and oblique velocity of Arabia in this area (Fig. 3).

322 In the Gulf of Aden, there is also a distinct change in the characteristics of the rift axis, approximately 400
323 km east to the triple junction region (Fig. 8). East to the Shukra al Sheik discontinuity, the Gulf of Aden is a
324 >2,000 m deep basin, which steeply deeps close to the shoreline. Along the basin, the axial trough is
325 fragmented by oblique left-lateral transform faults (Fig. 3). On the other hand, west to the Shukra al Sheik
326 discontinuity the basin is shallow (~700 m). In this section of the Gulf of Aden, the ~1,700 m deep and
327 ~400 km long curved axial trough impales the Afar triangle at the Gulf of Tadjoura (Djibouti) (Fig. 8). This
328 axial segment has a distinct gravity signature with 75 mGal central BGA peak and 20 – 35 Eotvos VGG side
329 peaks, and is characterized by the most intensive seismic activity, ~~perhaps the most intensive~~ in the rift
330 system, with over 1,000 recorded events with magnitudes > 4 ML (ISC catalog ; [Ruch et al., 2021](#)).

331 In the Main Ethiopian Rift, there are no abrupt changes in the morphology and trend of the rift valley in
332 the proximity to the Afar triangle (Fig. 9). Instead, the rift valley goes through an elevated dome peaking
333 approximately 400 km from the triple junction (Fig. 9a). The along-strike profile (profile B in Fig. 9) shows
334 that the rift valley reaches elevations of ~~more than~~ 2,000 m and is associated with a BGA low of -220
335 mGal.

336 In the Afar triangle, the morphology and VGG data indicate two distinguished regions of axial segments
337 (Fig. 10). (1) Southwest of the Tendaho-Goba'ad Discontinuity, a NE trending valley follows the NE trend
338 of the Main Ethiopian Rift, characterized by distinct central volcanoes along the axial depression (Fig. 3
339 and Fig. 10a). (2) Northeast of the Tendaho-Goba'ad Discontinuity, axial segments are composed of NW
340 trending short segments along volcanic ranges, parallel to the trend of the Red Sea

341 In summary, the rift axes of the Red Sea and the Gulf Aden drastically change their trend and morphological
342 characteristics ~400 km from the triple junction. In contrast, the trend and morphological characteristics
343 of the Main Ethiopian Rift are consistent from the Ethiopian highs up to the triple junction point in Afar.

344 7. Discussion

345 7.1. *The architecture of the intersection region*

346 The Afar triangle is the intersection region of three rift arms: the Gulf of Aden, the Red Sea, and the Main
347 Ethiopian Rift. Far from the intersection region, the architecture of the rifts, with rift margins parallel to
348 rift axes, suggest that rigid plate tectonics of the Nubian, Arabian, and Somalian plates controlled their
349 structural development (Garfunkel and Beyth, 2006; Reilinger et al., 2006; Reilinger and McClusky, 2011;
350 Schettino et al., 2018). However, the architecture of the intersection region is not simply resolved by rigid
351 plate kinematics (Garfunkel and Beyth, 2006). Our analysis points abrupt changes of the architectures of
352 the Gulf of Aden and of the Red Sea rifts, ~400 km from the triple junction. Here, the margins deviate from
353 their general orientation and show peaks in rift width (segments I to V in Fig. 5) and are not parallel to the
354 rift axes. The axes themselves deflect from their usual rift-parallel orientation and are curved towards the
355 direction of the triple junction as they meet the shoreline, forming bays (Fig 7 and Fig. 8). Within the Afar
356 triangle, northeast of the Tendaho-Goba'ad discontinuity, the margins are fragmented, and there are
357 multiple, short, and sub-parallel axial segments (Fig. 10).

358 Fig. 11 shows the mapped rift margins and axial segments. In this study, the term “mapped axial segments”
359 is not simply correlated with rift axes, especially in the onshore regions. The geology in this regions is quite
360 complex, including several fault and transfer zones, and, exposing pre-rift rock sequences (e.g., Varet,
361 2018), however, the mapped axial segments are somewhat correlative with rift axes that had been
362 suggested based on field observations (e.g., Rime et al., 2023).

363 Within the Afar triangle, southwest to the Tendaho-Goba’ad discontinuity, the rift margins are continuous
364 and smooth, and the axial volcanic range generally continues the trend of the axial valley of the Main
365 Ethiopian Rift, reflecting a sub-perpendicular extension in accordance with the Nubia –Somalia kinematics,
366 and thus, could be regarded as a rigid plate boundary.

367 Northeast of the Tendaho-Goba’ad discontinuity, axial segments are generally sub-parallel to the Red Sea
368 axis (Zwaan et al., 2020b), which led ~~to the interpretation of this region as authors-to-suggest-that-this~~
369 ~~region-reflects~~ an evolving discontinuity of the oceanic spreading center in the Red Sea (e.g. Tazieff et al.,
370 1972; Bosworth et al., 2005). Although several focal solutions indicated dextral strike-slip motions in this
371 area, we don’t find other evidence for a typical first-order transform connection between the ridge in the
372 Red Sea and the continuation of the northern Afar axial segments, offshore Gulf of Zula. Magnetic
373 isochrons in the Red Sea are mapped over 100 km south of the Gulf of Zula (Fig. 12), and the volcanic ridge
374 in the southern Red Sea is very active (Eyles et al., 2018). Although earthquake clusters at 16.5°N indicate
375 strike-slip solutions, supporting a structural connection to the Red Sea axis, these are abundant throughout
376 the study area (Hofstetter and Beyth, 2003). Alternatively, the jump between the Red Sea ridge and the
377 axial segments in northeastern Afar could be interpreted as a non-transform discontinuity, however,
378 second-order discontinuities are usually characterized by <30 km offsets, and here the jump is ~200 km
379 (Macdonald et al., 1984; Carbotte et al., 2016). Thus, there is no structural evidence to relate the axial
380 volcanism in the Afar triangle to the Red Sea spreading center. This conclusion agrees with the study of
381 Rime et al. (2023), which suggests a northward propagation of the rift in the Danakil Depression mainly
382 supported by younging trend of magmatic products, and rifting ages and other arguments.

383 The architecture of the intersection region northeast to the Tendaho-Goba’ad discontinuity reflects a
384 rugged connection of the Red Sea and the Gulf of Aden arms to the Main Ethiopian Rift and is characterized
385 by diffuse deformation rather than sharp plate boundaries. A recent model based on GPS observations
386 (Viltres et al., 2020) reveals a diffuse Danakil - Nubia boundary with inter-rifting deformation over > 100
387 km wide zone. The Danakil microplate extends to the Hanish-Zukur Islands at its southern edge (~13.8°N)
388 with no precise/sharp boundary (Fig. 3). The Danakil microplate is rotating counterclockwise (at a mean
389 rate of $1.5^\circ \pm 0.6^\circ/\text{Ma}$ for the last ~7 Ma ; Manighetti et al., 2001), while the Ali-Sabieh block, south of the
390 Gulf of Tadjoura, is rotating clockwise (15° between 8 to 4 Ma ; Audin et al., 2004), described as a “saloon-
391 doors” mode of opening (Fig. 11; Kidane, 2016).

392 The concept of segments of localized strain, which are spread over a broad zone in Afar was noted from
393 many indicators including diking events, structural geology, seismology and geodesy (Keir et al., 2011; Pagli
394 et al., 2014, 2018; Doubre et al., 2017). Analogue models demonstrated that the plate interactions in Afar
395 results in a broad zone of localized extension (Maestrelli et al., 2022).

396 Hence, the architecture of the intersection region of the rift arms discloses a ~150,000 km² complex region,
397 in which diffuse boundaries and microplate rotations link the three rift arms (Fig. 11). Accordingly, a
398 genuinely single triple junction point, in the sense of a three-rift arms intersection point, cannot be
399 specified for this system, and multiple triple junctions could be considered (e.g., see tectonic models in
400 Viltres et al., 2020). The difficulty of defining sharp plate boundaries within Afar was discussed in many

Commented [R11]: According to Wiktionary:
younging (uncountable):
1. (*geology*) The direction in which stratigraphy becomes
younger, for a particular formation

401 works (e.g., Barrberri and Varet, 1977 and references therein). Nevertheless, we agree that the intersection
402 point of the Ethiopian rift valley and the Tendaho-Goba'ad Discontinuity could be regarded as the 'main'
403 junction point of the rift system, as the deformation characteristics between the northern Main Ethiopian
404 Rift and the diffuse zone on the Gulf of Aden – Red Sea rifts are most distinctively changed there (Tsfaye
405 et al., 2003).

406 7.2. Spatial constraints in the development of the plume-rift system

407 The mapping of the rift margins and axial segments allows us to draw two spatial constraints in the
408 development of the plume-rift system:

409 (1) The first is the connection of the Main Ethiopian Rift to the Gulf of Aden - Red Sea rifts by a
410 northeastward propagation. Since the divergence between Nubia and Somalia is sub-perpendicular to the
411 strike of the northern Main Ethiopian Rift, its propagation direction is not entirely dictated by the
412 kinematics (Tsfaye et al., 2003; Wolfenden et al., 2004; Bonini et al., 2005; Keranen and Klemperer, 2008;
413 Abebe et al., 2010). The margins of southeast Afar show symmetric, continuous, and smooth curved
414 trends, from the elevated regions of the Main Ethiopian Rift to the Tendaho-Goba'ad Discontinuity (Fig.
415 5). With respect to the northeastward trend of the Main Ethiopian rift, the Somali margin is curved
416 clockwise, following the Ali-Sabieh sense of rotation (Kidane, 2016), whereas, the Ethiopian margin is
417 curved counterclockwise, like the Danakil sense of rotation (Fig. 11; Schult, 1974). This architecture could
418 be understood in terms of fracture mechanics by the reorientation of a propagating fracture near a pre-
419 existing fracture. Strain analysis indicates that a propagating fracture would curve parallel to the pre-
420 existing fracture under a tensional stress field due to free surface boundary conditions induced by the
421 open pre-existing fracture (Dyer, 1988). In analogy, the architecture of the study area express a smooth
422 linkage of the Main Ethiopian Rift to the pre-existing Gulf of Aden-Red Sea rifts by a northeastward
423 propagation. Hence, this implies that a triple junction formed at a late stage, when all three arms were
424 already significantly developed. This conclusion agrees with structural geochronology within the northern
425 Main Ethiopian Rift, showing that extension in the northern Main Ethiopian rift commenced at 11 Ma
426 (Wolfenden et al., 2004).

427 (2) The second spatial constraint is the abandonment of an early tectonic connection between the Red Sea
428 and the Gulf of Aden through the Bab al-Mandab Strait. As the VGG and neovolcanic activity indicate that
429 the Red Sea axis currently enters Afar at the Bay of Beylul (see section 6.2), we find arguments for an
430 earlier tectonic connection between the Red Sea and the Gulf of Aden through Bab al-Mandab Strait: (i)
431 South of 13.2°N and up to the connection to the Gulf of Aden (12.3°N), BGA and VGG depict the typical
432 and previously defined gravity signature of the rift axis (Fig. 7 and Fig. 8; see section 6.2). (ii) The submarine
433 channel north to the Hanish Island (Fig 7, 13.4°N) shows no association with modern water currents and
434 possibly formed by faults in the subsurface (Mitchell and Sofianos, 2018). (iii) This is the straight
435 continuation of the Red Sea axis, along which the basins are currtly connected (Fig. 1). Thus, it is reasonable
436 proposing that it was the tectonic connection in-durring the early stages of rift development. Likewise,
437 reconstructions suggest that the Danakil microplate started to rotate in the Middle Miocene (~10 Ma),
438 when Arabia was already separated from Africa (Collet et al., 2000; Schettino et al., 2016; Rime et al.,
439 2023). Those reconstructions show that the pre-Middle Miocene divergence was focused along Danakil
440 and Arabia at the southernmost Red Sea. This suggests that the present deflection of the rift axes at the
441 tip of the Gulf of Aden and the Red Sea marks a tectonic reorganization in this region.

442 Adopting the fracture propagation analog postulated here for the northeastward propagation of the Main
443 Ethiopian Rift, implies that the new stress conditions in Afar may be responsible for the abandonment of
444 the tectonic connection between the Red Sea and the Gulf of Aden. Rime et al. (2023) suggested that the
445 deposition of lacustrine sediments -(Chorora Fm) recorded marks the development of the Main Ethiopian
446 Rift in Afar. They point out that these sediments were deposited coeval with the individualization of the
447 Danakil Block, and thus to the decrease of the extensional tectonic activity at the southernmost Red Sea
448 rift.

449 These two spatial constraints suggest that the onset of the triple junction occurred at a late stage when
450 the three rift arms were already developed and the Red Sea was tectonically connected to the Gulf of
451 Aden, ~250 km away from the present-day triple junction (Fig. 13). The onset of the triple junction marked
452 a tectonic reorganization and microplate formation. As a result, the Gulf of Aden and the Red Sea arms are
453 not smoothly connected to the Main Ethiopian Rift, and a vast area of diffuse and complex deformation
454 developed within the intersection region.

455 7.3. Mechanisms for plume-rift association

456 The temporal constraints regarding the development of the plume-rift features, summarized in section 4,
457 together with the two spatial constraints inferred in this study, allow us to examine the causal relationship
458 between the activity of the Afar plume and rifting. Our insights suggest that neither 'active' nor 'passive'
459 rifting mechanisms are solely consistent with observations. Passive rifting models fail to explain the plume-
460 rift association mainly because the flood basalt volcanism cannot be attributed to a passively rising
461 asthenospheric mantle beneath a stretched and thinned lithosphere, as dynamic uplift in Ethiopia is a long-
462 lasting process that preceded flood basalt volcanism (Sembroni et al., 2016). Hence, rifting and associated
463 subsidence are subsequent to flood basalt volcanism (Fig. 4). The estimations that the Ethiopian plateau
464 was elevated ~1 km before flood basalts (Fig. 4) coincide with active plume-head predictions (Campbell
465 and Griffiths, 1990). Moreover, the passive model does not explain why a triple junction is located within
466 the flood basalts area, as rifting in the Red Sea and Gulf of Aden are at an oblique angle to the former
467 sutures (Buitter and Torsvik, 2014).

468 On the other hand, active models are not in line with the progressive development of the rifts, mainly
469 because the flood basalts region cannot be considered a center or a nucleus, from which rift arms spread,
470 as expected in an actively generated triple junction. Numerous studies noted that the tectonic
471 development of the Afar region is not compatible with a simplified model of rift arms that simultaneously
472 spread away from a triple junction (see Section 5.2 in Rime et al., 2023 for a review). The triple junction
473 was the last feature to develop in the system, by the propagation of the Main Ethiopian Rift towards Afar,
474 followed by a tectonic reorganization including the abandonment of a former tectonic connection
475 between the Red Sea and the Gulf of Aden. By this time, the rift arms had already developed, and the
476 break-up between Africa and Arabia had already been accomplished ~~between Africa and Arabia~~. This
477 tectonic reorganization cannot be attributed to the development of gravitational forces exerted by the
478 plume head (Hill, 1991), as it occurred ~20 Ma after flood basalts magmatism. That rules out the possibility
479 that the arrival of the Afar plume directly led to the formation of the triple junction and the rift arms did
480 not spread from the plume region.

481 We propose a scenario in which rifting was triggered by a plume-induced plate rotation (Fig. 2c). Numerical
482 simulations suggest that horizontal asthenospheric flows due to the arrival of a plume head at the base of
483 the lithosphere induce a plume-push force that can accelerate plates by several cm yr^{-1} (van Hinsbergen

484 et al., 2011, 2021; Pusok and Stegman, 2020). In this scenario, flood basalt volcanism would be
485 synchronous to an abrupt plate speed-up and thus to new remote stress conditions. In the case of the
486 Indian plate, at least two episodes of massive flood basalt volcanism, Morondava LIP (~94 Ma) and Deccan
487 traps (67 Ma), are associated with plume-derived plate acceleration, and a drastic change in the tectonic
488 framework (van Hinsbergen et al., 2011, 2021; Cande and Stegman, 2011; Pusok and Stegman, 2020).
489 Further, torque balance modeling simulating the horizontal forces generated from a point source (plume
490 head) suggests that horizontal plume-push can force a significant plate rotation and, consequently, initiate
491 new plate boundaries (van Hinsbergen et al., 2021).

492 In the Afro-Arabian rift, indeed new plate boundaries formed after the arrival of the large Afar plume and
493 a significant plate rotation of Arabia around a nearby pole characterizes the Arabian continent (Joffe and
494 Garfunkel, 1987; Viltres et al., 2022). Magnetic anomalies and structural reconstructions suggest that the
495 rotation around a nearby pole already characterized Arabia since the Oligocene (Fournier et al., 2010;
496 Schettino et al., 2018). Additionally, the beginning of intensive volcanism in the north-western Arabian
497 plate (Harrat Ash Shaam) at Late Oligocene (Ilani et al., 2001), reflected a change in mantle-crust
498 interaction and intracontinental extension within the Arabian plate, adjacent to the arrival of Afar plume
499 (Garfunkel, 1989). In the Harrat Ash Shaam volcanic field, diking directions from Miocene to recent ages
500 record the rotation of Arabia (Giannerini et al., 1988), suggesting that already during the first stages of
501 volcanism the Arabian plate was rotating around a nearby pole.

502 The arrival of the Afar plume was also accompanied by a slowdown of Africa (Le Pichon and Gaulier, 1988).
503 By this time, Africa collided with Eurasia in the west, explaining its slowdown (Jolivet and Faccenna, 2000)
504 and increased intraplate volcanism (Burke, 1996). However, this collision of Africa and Eurasia cannot
505 simply resolve the change in the rotation of Arabia as the Arabian continent collided with Eurasia not
506 earlier than ~18 Ma (Su and Zhou, 2020), although some authors suggested that asymmetrical along-
507 trench entrance of continental material could lead to an intraplate extension similar to those that
508 generated the Africa-Arabia break-up (Bellahsen et al., 2003). Faccenna et al. (2013) ~~already showed~~ that
509 plume-push from the Afar area resolves the present-day plate kinematics in the Middle East, particularly
510 the anti-clockwise toroidal pattern of the Arabia–Anatolia–Aegean system. The importance of active
511 upwelling in Afar to lateral mantle flow below Arabia is also illustrated by shear-wave splitting, indicating
512 a general N-S anisotropy in the mantle (Qaysi et al., 2018). Stamps et al. (2014) ~~calculated~~ the current
513 driving forces for the Nubia-Somalia divergence and found that gravitational potential energy is the most
514 significant force, stronger by an order of magnitude than forces from basal shear tractions of mantle
515 convection. They point out that the gravitational potential energy is sufficient to sustain present-day rifting
516 in East Africa but not to initiate rupture of continental lithosphere. In the case of the Arabian plate, basal
517 shear tractions are expected to be higher due to the orientation of northward-directed mantle flow
518 (Faccenna et al., 2013).

519 Plume-induced plate rotation settles the facts that regional uplift and flood basalt volcanism shortly
520 preceded rifting (Sembroni et al., 2016) together with the insight that rifting was developed by far field
521 forces and plate kinematics (Autin et al., 2013; Bosworth and Stockli, 2016). It also explains why the rifts
522 intersect within the plume region as the lithosphere in this region was weakened by the hot plume material
523 (François et al., 2018). Finally, it explains the delayed development of the Main Ethiopian Rift and the late
524 onset of the Afar triple junction by its northwestward propagation, as these were controlled by the slower
525 kinematics of the Somalian plate rather than dynamic forces. In this ~~tectonic scenario~~ manner, 'active' and
526 'passive' mechanisms are coupled and have positive feedback, allowing a close occurrence of flood basalt
527 volcanism and continental break-up, alongside passive rifting.

528 8. Summary and Conclusions

529 We reviewed the geologic setting of the Afro-Arabian rift, in which vast regions of flood basalts and
530 ongoing continental break-up are superimposed, aiming to infer a causal relationship between the activity
531 of the deep-seated Afar plume and crustal break-up. We explored the R-R-R triple junction between the
532 Gulf of Aden, the Red Sea, and the Main Ethiopian Rift that divides the large Cenozoic plume-related flood
533 basalt series in Ethiopia and Yemen. Based on ~~a synthesis and the~~ interpretation of topography,
534 bathymetry, and gravity, and the integration of magnetic anomalies, earthquakes, and volcano
535 distribution, we mapped the margins and axes of the rift arms.

536 Our results show that the terminations of the Gulf of Aden and the Red Sea arms are rough and irregular,
537 in contrast to the symmetric, continuous, and smooth architecture of the Main Ethiopian Rift. The triple
538 junction formed by the northeastward propagation of the Main Ethiopian Rift and the abandonment of
539 the tectonic connection between the Red Sea and the Gulf of Aden through Bab al-Mandab Strait. This
540 suggest a progressive development of a broad region of diffuse deformation at the intersection area. The
541 onset of the triple junction was the last feature to develop in the plume-rift system after all rift arms were
542 sufficiently evolved and the break-up between Africa and Arabia was already accomplished.

543 This progressive development does not align with the classic active rifting model, which predicts a plume-
544 generated triple junction at the locus of the rift development, from which the rifts develop. Nevertheless,
545 the classic passive rifting model fails to explain the chronological evidence, as flood basalts probably
546 erupted on elevated topography before rifting started. We discuss a scenario of plume-induced plate
547 rotation in which the arrival of the Afar plume triggered the rotation of Arabia around a nearby pole that
548 characterizes the system since the Oligocene. We argue that plume-induced plate rotation better explains
549 the progressive development of the plume-rift system in the Afro-Arabian rift.

550 9. Data availability

551 The bathymetry and topography data used in this study was retrieved from GEBCO Compilation Group
552 (2021), available at https://www.gebco.net/data_and_products/gridded_bathymetry_data/#area.

553 The VGG data used in this study is available at https://topex.ucsd.edu/grav_outreach/.

554 The BGA data used in this study is available at <http://icgem.gfz-potsdam.de/calgrid>; model XGM2019e-
555 2159, 'gravity_anomaly_bg'.

556 Earthquake data was retrieved from the International Seismological Centre (2020), On-line Bulletin,
557 <https://doi.org/10.31905/D808B830>.

558 Quaternary onshore volcano locations were retrieved from the Global Volcanism Program, Smithsonian
559 Institution, available at https://volcano.si.edu/volcanolist_holocene.cfm.

560 Magnetic anomalies data is available at
561 [https://figshare.com/articles/dataset/Transcurrent_Regimes_During_Rotational_Rifting_New_Insights_f
562 rom_Magnetic_Anomalies_in_the_Red_Sea/14743272](https://figshare.com/articles/dataset/Transcurrent_Regimes_During_Rotational_Rifting_New_Insights_from_Magnetic_Anomalies_in_the_Red_Sea/14743272).

563 10. Author contribution

564 RI carried out the study and wrote and revised the original draft of this paper. PH and NA provided
565 conceptual assistance, helped in writing and reviewed the manuscript. JE mentored the study, took care
566 of administration, and reviewed the manuscript.

567 11. Competing interests

568 The contact author has declared that neither of the authors has any competing interests.

569 12. Acknowledgments

570 This work was supported by the grants from Minerva Fellowship to R. I. We thank Neil Mitchell and
571 Valentin Rime for their helpful discussion throughout the open discussion process. We wish to thank
572 Antonio Schettino and Derek Keir for their review which helped improving the manuscript. We thank the
573 editors of Solid Earth for helpful comments and review process.

574 13. Figure captions

575 **Fig. 1.** Elevation map of the study area, showing the general plate tectonic configuration (from USGS and
576 from Viltres et al. (2020) in the Afar region) and Cenozoic volcanics (modified from Varet, 1978; Davison
577 et al., 1994; Beyene and Abdelsalam, 2005; Bosworth and Stockli, 2016) Black arrows indicate GPS
578 velocities in respect to Nubia (modified from Reilinger et al., 2006).

579 **Fig. 2.** Schematic mechanisms for plume-rift association in the Afro-Arabian rift. (a) Active mechanism
580 (e.g., Campbell and Griffiths, 1990). The plume head impinge and erode the base of the lithosphere, which
581 prompt uplift and decompression melting. These introduce internal extensional forces at the crust, leading
582 to break-up.. (b) Passive mechanism (e.g., White and McKenzie, 1989). Rifting is initiated solely by the
583 remote stresses, regardless of the underlying plume. In this mechanism, the production of massive
584 volcanism is allowed when the thinned and stretched lithosphere is underlaid by the thermal anomaly in
585 the mantle. Flood basalts volcanism is generated by decompression melting of the passively rising hot
586 asthenospheric mantle. (c) Plume-induced plate rotation (van Hinsbergen et al., 2021). Plume push forces
587 sourced by the drag of the flowing asthenosphere add up to the remote stresses to change the plate
588 kinematics. In this mechanism flood basalts volcanism is actively controlled, however, rifting is triggered
589 by the new plate kinematics.

590 **Fig. 3.** Map of the Afar region showing magnetic isochrons (modified from Fournier et al., 2010; Bridges et
591 al., 2012; Schettino et al., 2016), earthquake locations (from ISC catalog), Holocene onshore volcano
592 locations (from GVP catalog and Viltres et al. (2020)) and recent volcanism (modified from Keir et al., 2013).

593 **Fig. 4.** Elevation of the Ethiopian–Yemen plateau (grey boxes, after Sembroni et al., 2016; Faccenna et al.,
594 2019), volcanic episodes (orange and red bars) and opening rates of the rift arms (blue lines, modified
595 from Fournier et al., 2010; DeMets and Merkouriev, 2016; Schettino et al., 2018). Dashed lines indicate
596 estimations from geological observations and solid lines from magnetic anomalies.

597 **Fig. 5.** (a) Difference of Gaussians applied to topography and bathymetry showing rift margins (black lines).
598 White dashed lines indicate peaks in rift width. TGD is the Tendaho-Goba'ad Discontinuity. SSD is the
599 Shukra al Sheik discontinuity. Black dots indicate earthquake locations (ISC catalog). (b) Rift widths,
600 calculated in rift-perpendicular directions.

601 **Fig. 6.** Gravity data of the Afar region. (a) Vertical gravity gradient from Sandwell et al. (2014). Bouguer
602 anomaly model from ICGEM, XGM2019e (Zingerle et al., 2020).

603 **Fig. 7.** Bathymetry (a), vertical gravity gradient (b) and Bouguer anomaly (c) in the southern Red Sea. Black
604 dots indicate earthquake locations (ISC catalog). (d) Profiles across rift axis.

605 **Fig. 8.** Bathymetry (a), vertical gravity gradient (b) and Bouguer anomaly (c) in the Western Gulf of Aden.
606 Black dots indicate earthquake locations (ISC catalog). (d) Profiles across rift axis.

607 **Fig. 9.** Topography (a), vertical gravity gradient (b) and Bouguer anomaly (c) in the northern Main Ethiopian
608 Rift. Black dots indicate earthquake locations (ISC catalog). (d) Profiles across (AA') and along (BB') the rift
609 valley.

610 **Fig. 10.** Topography (a), vertical gravity gradient (b) and Bouguer anomaly (c) in the Afar triangle. Black
611 dots indicate earthquake locations (ISC catalog). TGD is the Tendaho-Goba'ad Discontinuity. (d) Profiles
612 SW (AA') and NE (BB') to the TGD.

613 **Fig. 11.** Rift margins (solid white lines) and axial segments (long dashed black lines) in the Afar region. Black
614 dots indicate earthquake locations (ISC catalog). TGD is the Tendaho-Goba'ad Discontinuity.

615 **Fig. 12.** Tilt-angle derivative map of magnetic anomalies, projected on a shaded relief after Issachar et al.
616 (2022). Purple colours represent positive angles and green colors represent negative angles. White dashed
617 lines indicate magnetic stripes (Schettino et al., 2016).

618 **Fig. 13.** Synthesis of the progressive development of the rift intersections.

619 14. References

- 620 Abebe, T., Balestrieri, M.L., and Bigazzi, G., 2010, The Central Main Ethiopian Rift is younger than 8 Ma:
621 confirmation through apatite fission-track thermochronology., doi:10.1111/j.1365-
622 3121.2010.00968.x.
- 623 Akram, F., Garcia, M.A., and Puig, D., 2017, Active contours driven by difference of Gaussians: Scientific
624 Reports, v. 7, p. 1–15, doi:10.1038/s41598-017-14502-w.
- 625 Anderson, D.L., 2005, Large Igneous Provinces, Delamination, and Fertile Mantle: Elements, v. 1, p. 271–
626 275, doi:10.2113/gselements.1.5.271.
- 627 Anderson, D.L., 1994, The sublithospheric mantle as the source of continental flood basalts; the case
628 against the continental lithosphere and plume head reservoirs: Earth and Planetary Science Letters,
629 v. 123, p. 269–280, doi:https://doi.org/10.1016/0012-821X(94)90273-9.
- 630 Audin, L., Quidelleur, X., Coulié, E., Courtillot, V., Gilder, S., Manighetti, I., Gillot, P.Y., Tapponnier, P., and
631 Kidane, T., 2004, Palaeomagnetism and K-Ar and 40 Ar/39 Ar ages in the Ali Sabieh area (Republic of
632 Djibouti and Ethiopia): Constraints on the mechanism of Aden ridge propagation into southeastern

633 Afar during the last 10 Myr: *Geophysical Journal International*, v. 158, p. 327–345,
634 doi:10.1111/j.1365-246X.2004.02286.x.

635 Augustin, N., van der Zwan, F.M., Devey, C.W., and Brandsdóttir, B., 2021, 13 million years of seafloor
636 spreading throughout the Red Sea Basin: *Nature Communications*, v. 12, p. 1–10,
637 doi:10.1038/s41467-021-22586-2.

638 Autin, J., Bellahsen, N., Leroy, S., Husson, L., Beslier, M.O., and d’Acremont, E., 2013, The role of structural
639 inheritance in oblique rifting: Insights from analogue models and application to the Gulf of Aden:
640 *Tectonophysics*, v. 607, p. 51–64, doi:10.1016/J.TECTO.2013.05.041.

641 Barrberi, F., and Varet, J., 1977, Volcanism of Afar: Small-scale plate tectonics implications: *GSA Bulletin*,
642 v. 88, p. 1251–1266, doi:10.1130/0016-7606(1977)88<1251:VOASPT>2.0.CO;2.

643 Bellahsen, N., Faccenna, C., Funiciello, F., Daniel, J.M., and Jolivet, L., 2003, Why did Arabia separate from
644 Africa? Insights from 3-D laboratory experiments: *Earth and Planetary Science Letters*, v. 216, p. 365–
645 381, doi:10.1016/S0012-821X(03)00516-8.

646 Bellahsen, N., Husson, L., Autin, J., Leroy, S., and D’Acremont, E., 2013, The effect of thermal weakening
647 and buoyancy forces on rift localization: Field evidences from the Gulf of Aden oblique rifting:
648 *Tectonophysics*, v. 607, p. 80–97, doi:10.1016/j.tecto.2013.05.042.

649 Bellieni, G., Visentin, E.J., Zanettin, B., Piccirillo, E.M., Radicati di Brozolo, F., and Rita, F., 1981, Oligocene
650 transitional tholeiitic magmatism in Northern turkana (Kenya): Comparison with the Coeval Ethiopian
651 volcanism: *Bulletin Volcanologique*, v. 44, p. 411–427, doi:10.1007/BF02600573.

652 Beyene, A., and Abdelsalam, M.G., 2005, Tectonics of the Afar Depression: A review and synthesis: *Journal*
653 *of African Earth Sciences*, v. 41, p. 41–59, doi:10.1016/j.jafrearsci.2005.03.003.

654 Bonini, M., Corti, G., Innocenti, F., Manetti, P., Mazzarini, F., Abebe, T., and Pecsckay, Z., 2005, Evolution of
655 the Main Ethiopian Rift in the frame of Afar and Kenya rifts propagation: v. 24,
656 doi:10.1029/2004TC001680.

657 Bosworth, W., 2015, Geological evolution of the Red Sea: historical background, review, and synthesis, *in*
658 *In The Red Sea*, Springer, Berlin, Heidelberg, p. 45–78, doi:10.1007/978-3-662-45201-1.

659 Bosworth, W., Huchon, P., and McClay, K., 2005, The Red Sea and Gulf of Aden Basins: *Journal of African*
660 *Earth Sciences*, v. 43, p. 334–378, doi:10.1016/j.jafrearsci.2005.07.020.

661 Bosworth, W., and Stockli, D.F., 2016, Early magmatism in the greater Red Sea rift: Timing and significance:
662 *Canadian Journal of Earth Sciences*, v. 53, p. 1158–1176, doi:10.1139/cjes-2016-0019.

663 Bridges, D.L., Mickus, K., Gao, S.S., Abdelsalam, M.G., and Alemu, A., 2012, Magnetic stripes of a
664 transitional continental rift in Afar: *Geology*, v. 40, p. 203–206, doi:10.1130/G32697.1.

665 Bryan, S.E., and Ferrari, L., 2013, Large igneous provinces and silicic large igneous provinces: Progress in
666 our understanding over the last 25 years: *GSA Bulletin*, v. 125, p. 1053–1078, doi:10.1130/B30820.1.

667 Buitert, S.J.H., and Torsvik, T.H., 2014, A review of Wilson Cycle plate margins: A role for mantle plumes in
668 continental break-up along sutures? *Gondwana Research*, v. 26, p. 627–653,
669 doi:10.1016/J.GR.2014.02.007.

670 Burke, K., 1996, The African Plate: *South African Journal of Geology*, v. 99, p. 341–409, doi:10.10520/EJC-
671 942801F20.

672 Burke, K., and Dewey, J.F., 1973, Plume-generated triple junctions: key indicators in applying plate
673 tectonics to old rocks: *The Journal of Geology*, v. 81, p. 406–433,

674 doi:<https://doi.org/10.1086/627882>.

675 Campbell, I.H., and Griffiths, R.W., 1990, Implications of mantle plume structure for the evolution of flood
676 basalts: *Earth and Planetary Science Letters*, v. 99, p. 79–93, doi:10.1016/0012-821X(90)90072-6.

677 Cande, S.C., and Stegman, D.R., 2011, Indian and African plate motions driven by the push force of the
678 Réunion plume head: *Nature*, v. 475, p. 47–52, doi:10.1038/nature10174.

679 Carbotte, S.M., Smith, D.K., Cannat, M., and Klein, E.M., 2016, Tectonic and magmatic segmentation of the
680 Global Ocean Ridge System: A synthesis of observations, *in* Geological Society Special Publication,
681 Geological Society of London, v. 420, p. 249–295, doi:10.1144/SP420.5.

682 Chatterjee, S., Goswami, A., and Scotese, C.R., 2013, The longest voyage: Tectonic, magmatic, and
683 paleoclimatic evolution of the Indian plate during its northward flight from Gondwana to Asia:
684 *Gondwana Research*, v. 23, p. 238–267, doi:10.1016/j.gr.2012.07.001.

685 Chorowicz, J., 2005, The East African rift system: *Journal of African Earth Sciences*, v. 43, p. 379–410,
686 doi:10.1016/j.jafrearsci.2005.07.019.

687 Collet, B., Taud, H., Parrot, J.F., Bonavia, F., and Chorowicz, J., 2000, A new kinematic approach for the
688 Danakil block using a Digital Elevation Model representation: *Tectonophysics*, v. 316, p. 343–357,
689 doi:10.1016/S0040-1951(99)00263-2.

690 Corti, G., 2009, Continental rift evolution: From rift initiation to incipient break-up in the Main Ethiopian
691 Rift, East Africa: *Earth-Science Reviews*, v. 96, p. 1–53, doi:10.1016/j.earscirev.2009.06.005.

692 Coulié, E., Quidelleur, X., Courtillot, V., Lefèvre, J.C., and Chiesa, S., 2003, Comparative K-Ar and Ar/Ar
693 dating of Ethiopian and Yemenite Oligocene volcanism: Implications for timing and duration of the
694 Ethiopian traps: *Earth and Planetary Science Letters*, v. 206, p. 477–492, doi:10.1016/S0012-
695 821X(02)01089-0.

696 Courtillot, V., Jaupart, C., Manighetti, I., Tapponnier, P., and Besse, J., 1999, On causal links between flood
697 basalts and continental breakup: *Earth and Planetary Science Letters*, v. 166, p. 177–195,
698 doi:10.1016/S0012-821X(98)00282-9.

699 Davison, I. et al., 1994, Geological evolution of the southeastern Red Sea Rift margin, Republic of Yemen:
700 *Geological Society of America Bulletin*, v. 106, p. 1474–1493, doi:10.1130/0016-
701 7606(1994)106<1474:GEOTSR>2.3.CO;2.

702 DeMets, C., and Merkouriev, S., 2016, High-resolution estimates of Nubia-Somalia plate motion since 20
703 Ma from reconstructions of the Southwest Indian Ridge, Red Sea and Gulf of Aden: *Geophysical
704 Journal International*, v. 207, p. 317–332, doi:10.1093/gji/ggw276.

705 Doubré, C. et al., 2017, Current deformation in Central Afar and triple junction kinematics deduced from
706 GPS and InSAR measurements: *Geophysical Journal International*, v. 208, p. 936–953,
707 doi:10.1093/gji/ggw434.

708 Duclaux, G., Huismans, R.S., and May, D.A., 2020, Rotation, narrowing, and preferential reactivation of
709 brittle structures during oblique rifting: *Earth and Planetary Science Letters*, v. 531, p. 115952,
710 doi:10.1016/j.epsl.2019.115952.

711 Dyer, R., 1988, Using joint interactions to estimate paleostress ratios: *Journal of Structural Geology*, v. 10,
712 p. 685–699, doi:10.1016/0191-8141(88)90076-4.

713 Ebinger, C.J., Keir, D., Bastow, I.D., Whaler, K., Hammond, J.O.S., Ayele, A., Miller, M.S., Tiberi, C., and
714 Hautot, S., 2017, Crustal Structure of Active Deformation Zones in Africa: Implications for Global
715 Crustal Processes: *Tectonics*, v. 36, p. 3298–3332, doi:<https://doi.org/10.1002/2017TC004526>.

716 Ernst, R.E., 2014, Large igneous provinces: Cambridge University Press.

717 Eyles, J.H.W., Illsley-Kemp, F., Keir, D., Ruch, J., and Jónsson, S., 2018, Seismicity Associated With the
718 Formation of a New Island in the Southern Red Sea: *Frontiers in Earth Science*, v. 6, p. 1–10,
719 doi:10.3389/feart.2018.00141.

720 Faccenna, C., Becker, T.W., Jolivet, L., and Keskin, M., 2013, Mantle convection in the Middle East:
721 Reconciling Afar upwelling, Arabia indentation and Aegean trench rollback: *Earth and Planetary
722 Science Letters*, v. 375, p. 254–269, doi:10.1016/J.EPSL.2013.05.043.

723 Faccenna, C., Glišović, P., Forte, A., Becker, T.W., Garzanti, E., Sembroni, A., and Gvirtzman, Z., 2019, Role
724 of dynamic topography in sustaining the Nile River over 30 million years: *Nature Geoscience*, v. 12,
725 p. 1012–1017, doi:10.1038/s41561-019-0472-x.

726 Forsyth, D., and Uyeda, S., 1975, On the relative importance of the driving forces of plate motion:
727 *Geophysical Journal International*, v. 43, p. 163–200.

728 Fournier, M. et al., 2010, Arabia-Somalia plate kinematics, evolution of the Aden-OwenCarlsberg triple
729 junction, and opening of the Gulf of Aden: *Journal of Geophysical Research: Solid Earth*, v. 115, p. 1–
730 24, doi:10.1029/2008JB006257.

731 François, T., Koptev, A., Cloetingh, S., Burov, E., and Gerya, T., 2018, Plume-lithosphere interactions in
732 rifted margin tectonic settings: Inferences from thermo-mechanical modelling: *Tectonophysics*, v.
733 746, p. 138–154, doi:10.1016/j.tecto.2017.11.027.

734 Frizon De Lamotte, D., Fourdan, B., Leleu, S., Leparmentier, F., and De Clarens, P., 2015, Style of rifting and
735 the stages of Pangea breakup: *Tectonics*, v. 34, p. 1009–1029, doi:10.1002/2014TC003760.

736 Fromm, T., Planert, L., Jokat, W., Ryberg, T., Behrmann, J.H., Weber, M.H., and Haberland, C., 2015, South
737 Atlantic opening: A plume-induced breakup? *Geology*, v. 43, p. 931–934, doi:10.1130/G36936.1.

738 Garfunkel, Z., 1989, Tectonic setting of phanerozoic magmatism in Israel: *Israel journal of earth-sciences*,
739 v. 38, p. 51–74.

740 Garfunkel, Z., and Beyth, M., 2006, Constraints on the structural development of Afar imposed by the
741 kinematics of the major surrounding plates: *Geological Society Special Publication*, v. 259, p. 23–42,
742 doi:10.1144/GSL.SP.2006.259.01.04.

743 Gass, I.G., Mallick, D.I.J., and Cos, K.G., 1973, Volcanic islands of the Red Sea: *Journal of the Geological
744 Society*, v. 129, p. 275–309, doi:10.1144/gsjgs.129.3.0275.

745 GEBCO Compilation Group, 2021, The GEBCO_2019 Grid: a continuous terrain model of the global oceans
746 and land:, doi:10.5285/c6612cbe-50b3-0cff-e053-6c86abc09f8f.

747 Geoffroy, L., 2005, Volcanic passive margins: *Comptes Rendus Geoscience*, v. 337, p. 1395–1408,
748 doi:10.1016/J.CRTE.2005.10.006.

749 George, R., Rogers, N., and Kelley, S., 1998, Earliest magmatism in Ethiopia: Evidence for two mantle
750 plumes in one flood basalt province: *Geology*, v. 26, p. 923–926, doi:10.1130/0091-
751 7613(1998)026<0923:EMIEEF>2.3.CO;2.

752 Giannerini, G., Campredon, R., Feraud, G., and Abou Zakhem, B., 1988, Deformations intraplaques et
753 volcanisme associe; exemple de la bordure NW de la plaque Arabique au Cenozoique: *Bulletin de la
754 Société Géologique de France*, v. IV, p. 937–947, doi:10.2113/gssgfbull.IV.6.937.

755 Gillard, M., Leroy, S., Cannat, M., and Sloan, H., 2021, Margin-to-Margin Seafloor Spreading in the Eastern
756 Gulf of Aden: A 16 Ma-Long History of Deformation and Magmatism from Seismic Reflection, Gravity

757 and Magnetic Data: *Frontiers in Earth Science*, v. 9, p. 628, doi:10.3389/feart.2021.707721.

758 Girdler, R. W., and Styles, P. (1974). Two stage Red Sea floor spreading. *Nature*, 247(5435), 7-11, doi:
759 10.1038/247007a0.

760 Gvirtzman, Z., Faccenna, C., and Becker, T.W., 2016, Isostasy, flexure, and dynamic topography:
761 *Tectonophysics*, v. 683, p. 255–271, doi:10.1016/j.tecto.2016.05.041.

762 Hill, R.I., 1991, Starting plumes and continental break-up: *Earth and Planetary Science Letters*, v. 104, p.
763 398–416, doi:10.1016/0012-821X(91)90218-7.

764 van Hinsbergen, D.J.J. et al., 2021, A record of plume-induced plate rotation triggering subduction
765 initiation: *Nature Geoscience*, v. 14, p. 626–630, doi:10.1038/s41561-021-00780-7.

766 van Hinsbergen, D.J.J., Steinberger, B., Doubrovine, P. V., and Gassmüller, R., 2011, Acceleration and
767 deceleration of India-Asia convergence since the Cretaceous: Roles of mantle plumes and continental
768 collision: *Journal of Geophysical Research: Solid Earth*, v. 116, p. 6101, doi:10.1029/2010JB008051.

769 Hofstetter, R., and Beyth, M., 2003, The afar depression: Interpretation of the 1960-2000 earthquakes:
770 *Geophysical Journal International*, v. 155, p. 715–732, doi:10.1046/j.1365-246X.2003.02080.x.

771 Hughes, G.W., Varol, O., and Beydoun, Z.R., 1991, Evidence for Middle Oligocene rifting of the Gulf of Aden
772 and for Late Oligocene rifting of the southern Red Sea: *Marine and Petroleum Geology*, v. 8, p. 354–
773 358, doi:10.1016/0264-8172(91)90088-I.

774 Huismans, R.S., Podladchikov, Y.Y., and Cloetingh, S., 2001, Transition from passive to active rifting:
775 Relative importance of asthenospheric doming and passive extension of the lithosphere: *Journal of*
776 *Geophysical Research: Solid Earth*, v. 106, p. 11271–11291, doi:10.1029/2000JB900424.

777 Ilani, S., Harlavan, Y., Tarawneh, K., Rabba, I., Weinberger, R., Ibrahim, K., Peltz, S., and Steinitz, G., 2001,
778 New K-Ar ages of basalts from the Harrat Ash Shaam volcanic field in Jordan: Implications for the
779 span and duration of the upper-mantle upwelling beneath the western Arabian plate: *Geology*, v. 29,
780 p. 171–174, doi:10.1130/0091-7613(2001)029<0171:NKAAOB>2.0.CO;2.

781 Ince, E.S., Barthelmes, F., Reißland, S., Elger, K., Förste, C., Flechtner, F., and Schuh, H., 2019, ICGEM – 15
782 years of successful collection and distribution of global gravitational models, associated services, and
783 future plans: *Earth System Science Data*, v. 11, p. 647–674, doi:10.5194/essd-11-647-2019.

784 Issachar, R., Ebbing, J., and Dilixiati, Y., 2022, New magnetic anomaly map for the Red Sea reveals
785 transtensional structures associated with rotational rifting: *Scientific Reports*, v. 12, p. 1–13,
786 doi:10.1038/s41598-022-09770-0.

787 Ivanov, A. V., Demonterova, E.I., He, H., Perepelov, A.B., Travin, A. V., and Lebedev, V.A., 2015, Volcanism
788 in the Baikal rift: 40years of active-versus-passive model discussion: *Earth-Science Reviews*, v. 148,
789 p. 18–43, doi:10.1016/j.earscirev.2015.05.011.

790 Joffe, S., and Garfunkel, Z., 1987, Plate kinematics of the Red Sea – a re-evaluation: *Tectonophysics*, v. 141,
791 p. 5–22.

792 Jolivet, L., and Faccenna, C., 2000, Mediterranean extension and the Africa-Eurasia collision: *Tectonics*, v.
793 19, p. 1095–1106, doi:10.1029/2000TC900018.

794 Keen, C.E., 1985, The dynamics of rifting: deformation of the lithosphere by active and passive driving
795 forces: *Geophys. J. R. astr. Soc.*, v. 80, p. 95–120,
796 <https://academic.oup.com/gji/article/80/1/95/610547> (accessed August 2021).

797 Keir, D., Bastow, I.D., Pagli, C., and Chambers, E.L., 2013, The development of extension and magmatism

798 in the Red Sea rift of Afar: *Tectonophysics*, v. 607, p. 98–114, doi:10.1016/j.tecto.2012.10.015.

799 Keir, D., Pagli, C., Bastow, I.D., and Ayele, A., 2011, The magma-assisted removal of Arabia in Afar: Evidence
800 from dike injection in the Ethiopian rift captured using InSAR and seismicity: *Tectonics*, v. 30,
801 doi:https://doi.org/10.1029/2010TC002785.

802 Keranen, K., and Klemperer, S.L., 2008, Discontinuous and diachronous evolution of the Main Ethiopian
803 Rift : Implications for development of continental rifts: *Earth and Planetary Science Letters*, v. 265, p.
804 96–111, doi:10.1016/j.epsl.2007.09.038.

805 Kidane, T., 2016, Strong clockwise block rotation of the Ali-Sabieh/Aisha Block: Evidence for opening of the
806 Afar Depression by a “saloon-door” mechanism, *in* Geological Society Special Publication, Geological
807 Society of London, v. 420, p. 209–219, doi:10.1144/SP420.10.

808 Koppers, A.A.P., Becker, T.W., Jackson, M.G., Konrad, K., Müller, R.D., Romanowicz, B., Steinberger, B., and
809 Whittaker, J.M., 2021, Mantle plumes and their role in Earth processes: *Nature Reviews Earth &*
810 *Environment*, v. 2, p. 382–401, doi:10.1038/s43017-021-00168-6.

811 Koptev, A., Gerya, T., Calais, E., Leroy, S., and Burov, E., 2018, Afar triple junction triggered by plume-
812 assisted bi-directional continental break-up: *Scientific Reports*, v. 8, p. 1–7, doi:10.1038/s41598-018-
813 33117-3.

814 Leroy, S. et al., 2013, From rifting to oceanic spreading in the Gulf of Aden: A synthesis: *Frontiers in Earth*
815 *Sciences*, v. 5, p. 385–427, doi:10.1007/978-3-642-30609-9_20.

816 Lithgow-Bertelloni, C., and Silver, P.G., 1998, Dynamic topography, plate driving forces and the African
817 superswell: *Nature*, v. 395, p. 269–272, doi:10.1038/26212.

818 Macdonald, K., Sempere, J.C., and Fox, P.J., 1984, East Pacific Rise from Siqueiros to Orozco fracture zones:
819 along- strike continuity of axial neovolcanic zone and structure and evolution of overlapping
820 spreading centers.: *Journal of Geophysical Research*, v. 89, p. 6049–6069,
821 doi:10.1029/JB089iB07p06049.

822 Maestrelli, D., Brune, S., Corti, G., Keir, D., Muluneh, A.A., and Sani, F., 2022, Analog and Numerical
823 Modeling of Rift-Rift-Rift Triple Junctions: *Tectonics*, v. 41, p. e2022TC007491,
824 doi:https://doi.org/10.1029/2022TC007491.

825 Manighetti, I., Tapponnier, P., Courtillot, V., Gallet, Y., Jacques, E., and Gillot, P.Y., 2001, Strain transfer
826 between disconnected, propagating rifts in Afar: *Journal of Geophysical Research: Solid Earth*, v. 106,
827 p. 13613–13665, doi:10.1029/2000jb900454.

828 Mattash, M.A., Pinarelli, L., Vaselli, O., Minissale, A., Al-Kadasi, M., Shawki, M.N., and Tassi, F., 2013,
829 Continental Flood Basalts and Rifting: Geochemistry of Cenozoic Yemen Volcanic Province:
830 *International Journal of Geosciences*, v. 04, p. 1459–1466, doi:10.4236/ijg.2013.410143.

831 McConnell, R., and Baker, B., 1970, The Structural Pattern of the Afro-Arabian Rift System in Relation to
832 Plate Tectonics: Discussion: *Philosophical Transactions of the Royal Society of London Series A*, v.
833 267, p. 390–391, https://www.jstor.org/stable/73628?seq=3#metadata_info_tab_contents
834 (accessed August 2021).

835 McDougall, I. an, and Brown, F.H., 2009, Timing of volcanism and evolution of the northern Kenya Rift:
836 *Geological Magazine*, v. 146, p. 34–47, doi:DOI: 10.1017/S0016756808005347.

837 Meshesha, D., and Shinjo, R., 2008, Rethinking geochemical feature of the Afar and Kenya mantle plumes
838 and geodynamics implications: *Journal of Geophysical Research: Solid Earth*, v. 113, p. 9209,
839 doi:10.1029/2007JB005549.

840 Mitchell, N.C., and Bosworth, (in press), W. The tectonic stability of Arabia, *in* Rasul, N.M.A. and Stewart,
841 I.C.F. eds., The tectonic stability of Arabia, in Rifting and sediments in the Red Sea and Arabian Gulf
842 regions, Taylor & Francis.

843 Mitchell, N.C., and Sofianos, S.S., 2018, Origin of submarine channel north of hanish sill, red sea, *in*
844 Geological Setting, Palaeoenvironment and Archaeology of the Red Sea, Springer International
845 Publishing, p. 259–273, doi:10.1007/978-3-319-99408-6_12.

846 Mitra, S., Mitra, K., Gupta, S., Bhattacharya, S., Chauhan, P., and Jain, N., 2017, Alteration and submergence
847 of basalts in Kachchh, Gujarat, India: implications for the role of the Deccan Traps in the India–
848 Seychelles break-up: Geological Society, London, Special Publications, v. 445, p. 47–67,
849 doi:10.1144/SP445.9.

850 Morag, N., Haviv, I., Eyal, M., Kohn, B.P., and Feinstein, S., 2019, Early flank uplift along the Suez Rift:
851 Implications for the role of mantle plumes and the onset of the Dead Sea Transform: Earth and
852 Planetary Science Letters, v. 516, p. 56–65, doi:10.1016/j.epsl.2019.03.002.

853 Moretti, I., and Froidevaux, C., 1986, Thermomechanical models of active rifting: Tectonics, v. 5, p. 501–
854 511, doi:10.1029/TC0051004P00501.

855 Morgan, W.J., 1971, Convection plumes in the lower mantle: Nature, v. 230, p. 42–43,
856 doi:10.1038/230042a0.

857 Okwokwo, O.I., Mitchell, N.C., Shi, W., Stewart, I.C.F., and Izzeldin, A.Y., 2022, How have thick evaporites
858 affected early seafloor spreading magnetic anomalies in the Central Red Sea? Geophysical Journal
859 International, v. 229, p. 1550–1566, doi:10.1093/gji/ggac012.

860 Pagli, C., Wang, H., Wright, T.J., Calais, E., and Lewi, E., 2014, Current plate boundary deformation of the
861 Afar rift from a 3-D velocity field inversion of InSAR and GPS: Journal of Geophysical Research: Solid
862 Earth, v. 119, p. 8562–8575, doi:https://doi.org/10.1002/2014JB011391.

863 Pagli, C., Yun, S.-H., Ebinger, C., Keir, D., and Wang, H., 2018, Strike-slip tectonics during rift linkage:
864 Geology, v. 47, p. 31–34, doi:10.1130/G45345.1.

865 Peate, I.U., Baker, J.A., Al-Kadasi, M., Al-Subbary, A., Knight, K.B., Riisager, P., Thirlwall, M.F., Peate, D.W.,
866 Renne, P.R., and Menzies, M.A., 2005, Volcanic stratigraphy of large-volume silicic pyroclastic
867 eruptions during Oligocene Afro-Arabian flood volcanism in Yemen: Bulletin of Volcanology, v. 68, p.
868 135–156, doi:10.1007/s00445-005-0428-4.

869 Le Pichon, X., and Gaulier, J.-M., 1988, The rotation of Arabia and the Levant fault system: Tectonophysics,
870 v. 153, p. 271–294, doi:10.1016/0040-1951(88)90020-0.

871 Plaziat, J.-C., Baltzer, F., Choukri, A., Conchon, O., Freytet, P., Orszag-Sperber, F., Raguideau, A., and Reyss,
872 J.-L., 1998, Quaternary marine and continental sedimentation in the northern Red Sea and Gulf of
873 Suez (Egyptian coast): influences of rift tectonics, climatic changes and sea-level fluctuations, *in*
874 Sedimentation and Tectonics in Rift Basins Red Sea:- Gulf of Aden, Springer Netherlands, p. 537–573,
875 doi:10.1007/978-94-011-4930-3_29.

876 Prave, A.R., Bates, C.R., Donaldson, C.H., Toland, H., Condon, D.J., Mark, D., and Raub, T.D., 2016, Geology
877 and geochronology of the Tana Basin, Ethiopia: LIP volcanism, Super eruptions and Eocene-Oligocene
878 environmental change: Earth and Planetary Science Letters, v. 443, p. 1–8,
879 doi:10.1016/j.epsl.2016.03.009.

880 Pusok, A.E., and Stegman, D.R., 2020, The convergence history of India-Eurasia records multiple
881 subduction dynamics processes: Science Advances, v. 6,

882 doi:10.1126/SCIADV.AAZ8681/SUPPL_FILE/AAZ8681_SM.PDF.

883 Qaysi, S., Liu, K.H., and Gao, S.S., 2018, A Database of Shear-Wave Splitting Measurements for the Arabian
884 Plate: *Seismological Research Letters*, v. 89, p. 2294–2298, doi:10.1785/0220180144.

885 Reilinger, R. et al., 2006, GPS constraints on continental deformation in the Africa-Arabia-Eurasia
886 continental collision zone and implications for the dynamics of plate interactions: *Journal of*
887 *Geophysical Research-Solid Earth*, v. 111.

888 Reilinger, R., and McClusky, S., 2011, Nubia-Arabia-Eurasia plate motions and the dynamics of
889 Mediterranean and Middle East tectonics: *Geophysical Journal International*, v. 186, p. 971–979,
890 doi:10.1111/j.1365-246X.2011.05133.x.

891 Richards, M.A., Duncan, R.A., and Courtillot, V.E., 1989, Flood basalts and hot-spot tracks: Plume heads
892 and tails: *Science*, v. 246, p. 103–107, doi:10.1126/science.246.4926.103.

893 Rime, V., Foubert, A., Ruch, J., and Kidane, T., 2023, Tectonostratigraphic evolution and significance of the
894 Afar Depression: *Earth-Science Reviews*, v. 244, p. 104519,
895 doi:https://doi.org/10.1016/j.earscirev.2023.104519.

896 Roger, J., Platel, J.P., Cavelier, C., and Bourdillon-de-Grissac, C., 1989, Données nouvelles sur la
897 stratigraphie et l'histoire géologique du Dhofar (Sultanat d'Oman): *Bulletin de la Société géologique*
898 *de France*, v. 2, p. 256–277, In France, abstract in English.

899 Rooney, T.O., 2017, The Cenozoic magmatism of East-Africa: Part I — Flood basalts and pulsed magmatism:
900 *Lithos*, v. 286–287, p. 264–301, doi:10.1016/j.lithos.2017.05.014.

901 [Ruch, J., Keir, D., Passarelli, L., Di Giacomo, D., Ogubazghi, G., and Jónsson, S., 2021, Revealing 60 years of](#)
902 [Earthquake Swarms in the Southern Red Sea, Afar and the Gulf of Aden: *Frontiers in Earth Science*,](#)
903 [v. 9, p. 690, doi:10.3389/feart.2021.664673.](#)

904 Sandwell, D.T., Müller, R.D., Smith, W.H.F., Garcia, E., and Francis, R., 2014, New global marine gravity
905 model from CryoSat-2 and Jason-1 reveals buried tectonic structure: *Science*, v. 346, p. 65–67,
906 doi:10.1126/SCIENCE.1258213.

907 Schettino, A., Macchiavelli, C., Pierantoni, P.P., Zanoni, D., and Rasul, N., 2016, Recent kinematics of the
908 tectonic plates surrounding the red sea and gulf of aden: *Geophysical Journal International*, v. 207,
909 p. 457–480, doi:10.1093/gji/ggw280.

910 Schettino, A., Macchiavelli, C., and Rasul, N.M.A., 2018, Plate motions around the red sea since the early
911 oligocene, *in Geological Setting, Palaeoenvironment and Archaeology of the Red Sea*, Springer
912 International Publishing, p. 203–220, doi:10.1007/978-3-319-99408-6_9.

913 Schult, A., 1974, Palaeomagnetism of tertiary volcanic rocks from the Ethiopian southern plateau and the
914 Danakil block: *Journal of Geophysics*, v. 40, p. 203–212,
915 <https://journal.geophysicsjournal.com/JofG/article/view/277> (accessed June 2021).

916 Sembroni, A., Faccenna, C., Becker, T.W., Molin, P., and Abebe, B., 2016, Long-term, deep-mantle support
917 of the Ethiopia-Yemen Plateau: *Tectonics*, v. 35, p. 469–488, doi:10.1002/2015TC004000.Received.

918 Sengör, A.M.C., and Burke, K., 1978, Relative timing of rifting and volcanism on Earth and its tectonic
919 implications: *Geophysical Research Letters*, v. 5, p. 419–421, doi:10.1029/GL005I006P00419.

920 Sobolev, S. V., Sobolev, A. V., Kuzmin, D. V., Krivolutsкая, N.A., Petrunin, A.G., Arndt, N.T., Radko, V.A.,
921 and Vasiliev, Y.R., 2011, Linking mantle plumes, large igneous provinces and environmental
922 catastrophes: *Nature*, v. 477, p. 312–316, doi:10.1038/nature10385.

- 923 Stamps, D.S., Flesch, L.M., Calais, E., and Ghosh, A., 2014, Current kinematics and dynamics of Africa and
 924 the East African Rift System: *Journal of Geophysical Research: Solid Earth*, v. 119, p. 5161–5186,
 925 doi:10.1002/2013JB010717.
- 926 Stockli, D.F., and Bosworth, W.B., 2018, Timing of extensional faulting along the magma-poor central and
 927 northern red sea rift margin-transition from regional extension to necking along a hyperextended
 928 rifted margin, *in Geological Setting, Palaeoenvironment and Archaeology of the Red Sea*, Springer
 929 International Publishing, p. 81–111, doi:10.1007/978-3-319-99408-6_5.
- 930 Su, H., and Zhou, J., 2020, Timing of Arabia-Eurasia collision: Constraints from restoration of crustal-scale
 931 cross-sections: *Journal of Structural Geology*, v. 135, p. 104041, doi:10.1016/j.jsg.2020.104041.
- 932 Szymanski, E., Stockli, D.F., Johnson, P.R., and Hager, C., 2016, Thermochronometric evidence for diffuse
 933 extension and two-phase rifting within the Central Arabian Margin of the Red Sea Rift: *Tectonics*, v.
 934 35, p. 2863–2895, doi:10.1002/2016TC004336.
- 935 Tazieff, H.T., Varet, J., Barberi, F., and Giglia, G., 1972, Tectonic significance of the Afar (or Danakil)
 936 depression: *Nature*, v. 235, p. 144–147.
- 937 Tesfaye, S., Harding, D.J., and Kusky, T.M., 2003, Early continental breakup boundary and migration of the
 938 Afar triple junction, Ethiopia: *Bulletin of the Geological Society of America*, v. 115, p. 1053–1067,
 939 doi:10.1130/B25149.1.
- 940 Varet, J., 2018, *Geology of Afar (East Africa)*: 1–249 p.
- 941 Varet, J., 1978, *Geology of central and southern Afar (Ethiopia and Djibouti Republic)*: Paris, Centre
 942 national de la recherche scientifique.
- 943 Viltres, R., Jónsson, S., Alothman, A.O., Liu, S., Leroy, S., Masson, F., Doubre, C., and Reilinger, R., 2022,
 944 Present-Day Motion of the Arabian Plate: *Tectonics*, v. 41, p. e2021TC007013,
 945 doi:https://doi.org/10.1029/2021TC007013.
- 946 Viltres, R., Jónsson, S., Ruch, J., Doubre, C., Reilinger, R., Floyd, M., and Ogubazghi, G., 2020, Kinematics
 947 and deformation of the southern Red Sea region from GPS observations: *Geophysical Journal
 948 International*, v. 221, p. 2143–2154, doi:10.1093/gji/ggaa109.
- 949 Watchorn, F., Nichols, G.J., and Bosence, D.W.J., 1998, Rift-related sedimentation and stratigraphy,
 950 southern Yemen (Gulf of Aden), *in Sedimentation and Tectonics in Rift Basins Red Sea:- Gulf of Aden*,
 951 Springer Netherlands, p. 165–189, doi:10.1007/978-94-011-4930-3_11.
- 952 Wescott, W.A., Wigger, S.T., Stone, D.M., and Morley, C.K., 1999, *AAPG Studies in Geology# 44, Chapter 3:*
 953 *Geology and Geophysics of the Lotikipi Plain*:
- 954 White, R., and McKenzie, D., 1989, Magmatism at rift zones: the generation of volcanic continental margins
 955 and flood basalts: *Journal of Geophysical Research*, v. 94, p. 7685–7729,
 956 doi:10.1029/JB094iB06p07685.
- 957 White, R.S., and McKenzie, D., 1995, Mantle plumes and flood basalts: *Journal of Geophysical Research*, v.
 958 100, p. 543–560, doi:10.1029/95jb01585.
- 959 Will, T.M., and Frimmel, H.E., 2018, Where does a continent prefer to break up? Some lessons from the
 960 South Atlantic margins: *Gondwana Research*, v. 53, p. 9–19, doi:10.1016/j.gr.2017.04.014.
- 961 Wilson, J.T., 1963, A possible origin of the Hawaiian Islands: *Canadian Journal of Physics*, v. 41, p. 863–870,
 962 doi:10.1139/P63-094.
- 963 Wolfenden, E., Ebinger, C., Yirgu, G., Deino, A., and Ayalew, D., 2004, Evolution of the northern Main

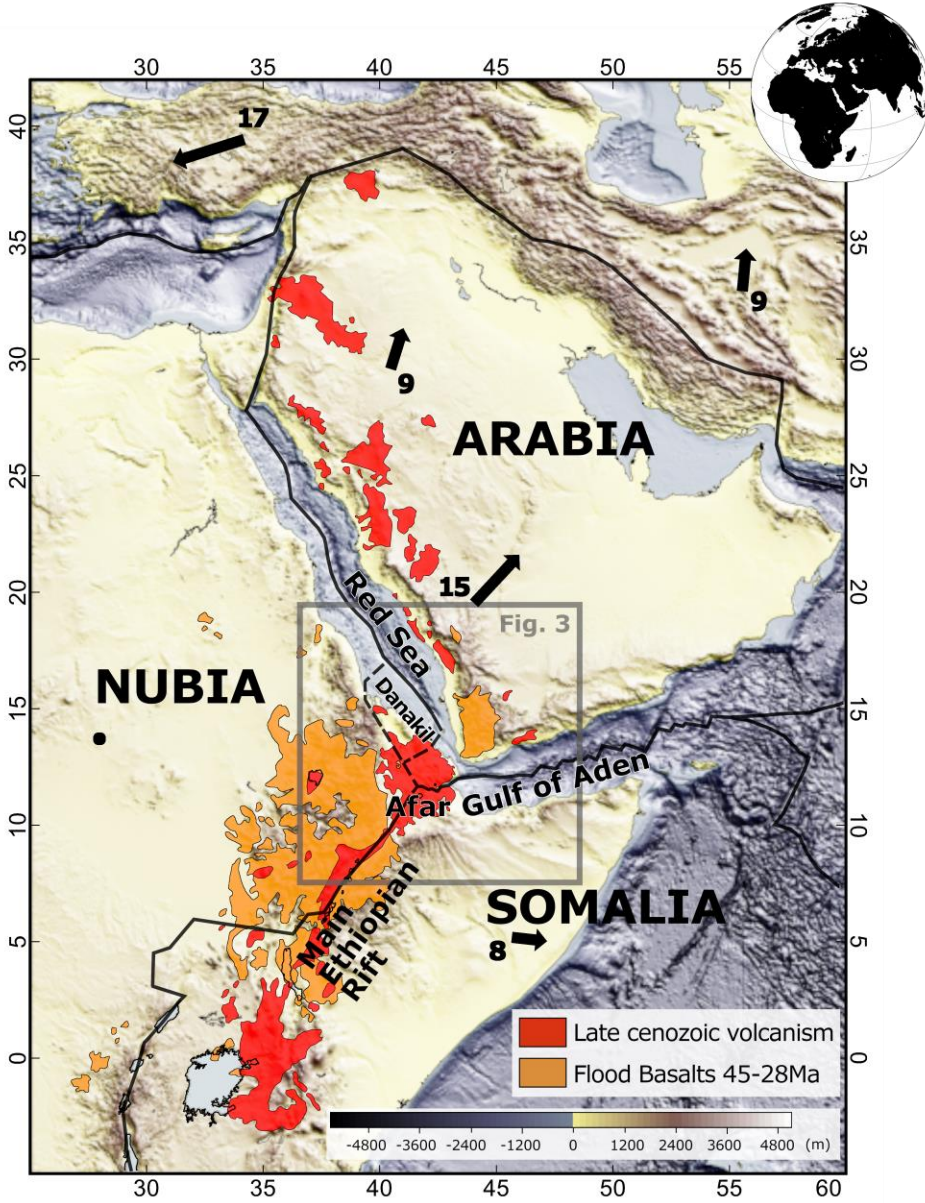
964 Ethiopian rift: Birth of a triple junction: *Earth and Planetary Science Letters*, v. 224, p. 213–228,
965 doi:10.1016/j.epsl.2004.04.022.

966 Zingerle, P., Pail, R., Gruber, T., and Oikonomidou, X., 2020, The combined global gravity field model
967 XGM2019e: *Journal of Geodesy* 2020 94:7, v. 94, p. 1–12, doi:10.1007/S00190-020-01398-0.

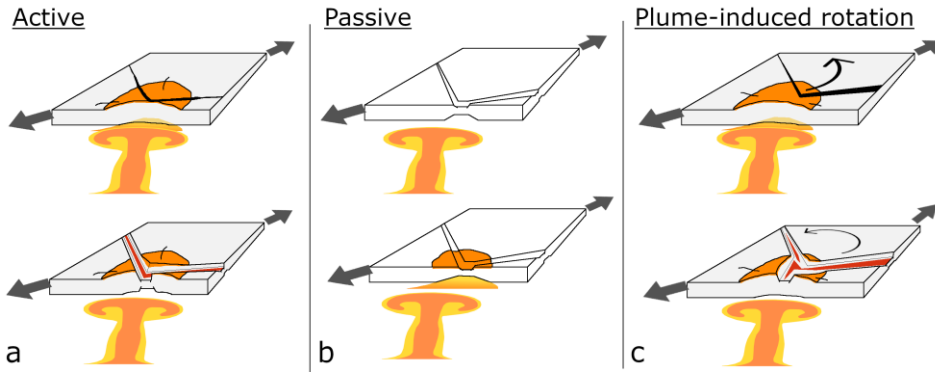
968 Zwaan, F., Corti, G., Keir, D., and Sani, F., 2020a, A review of tectonic models for the rifted margin of Afar:
969 Implications for continental break-up and passive margin formation: *Journal of African Earth*
970 *Sciences*, v. 164, doi:10.1016/j.jafrearsci.2019.103649.

971 Zwaan, F., Corti, G., Sani, F., Keir, D., Muluneh, A.A., Illsley-Kemp, F., and Papini, M., 2020b, Structural
972 Analysis of the Western Afar Margin, East Africa: Evidence for Multiphase Rotational Rifting:
973 *Tectonics*, v. 39, doi:10.1029/2019TC006043.

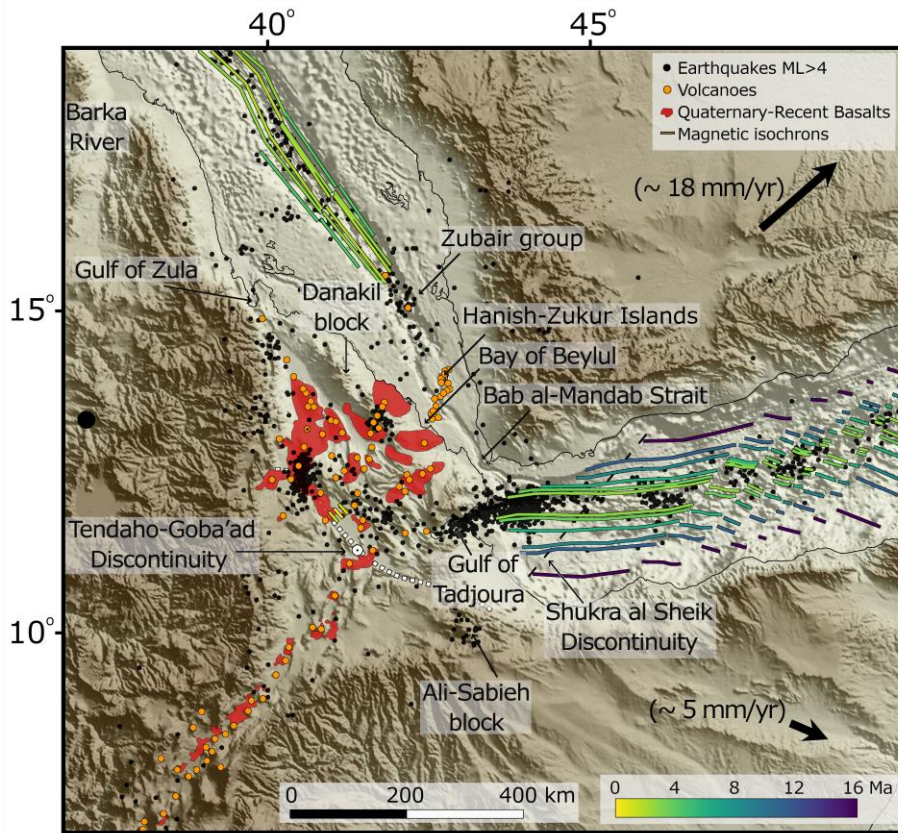
974



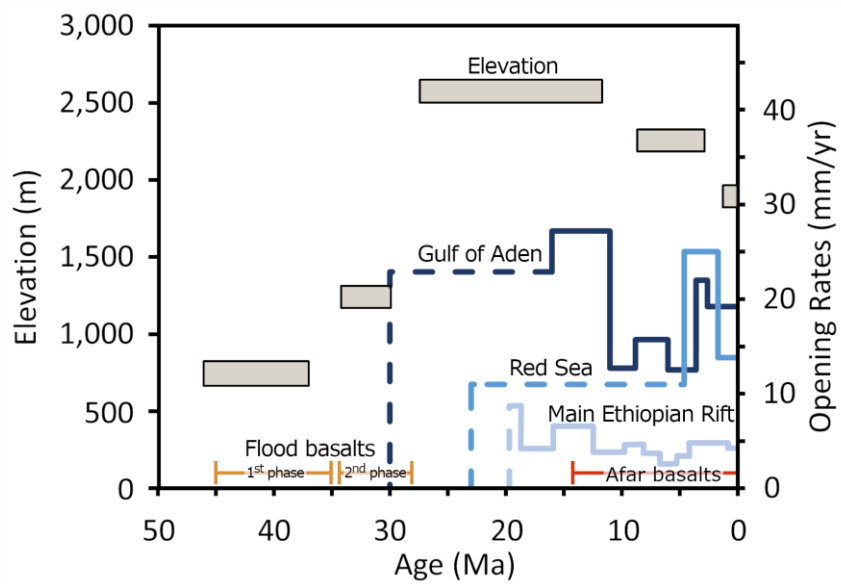
976
977 Fig. 1.



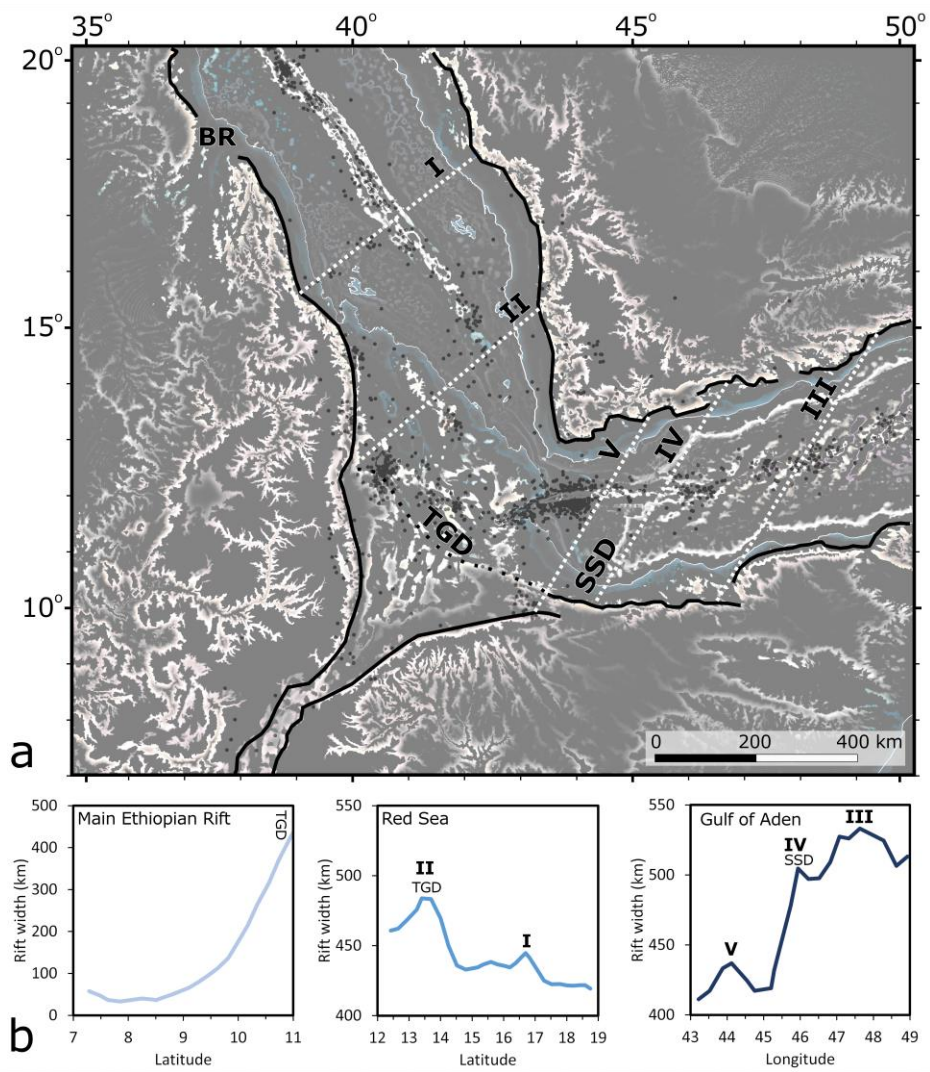
978
979 Fig. 2.



980
981 Fig. 3.

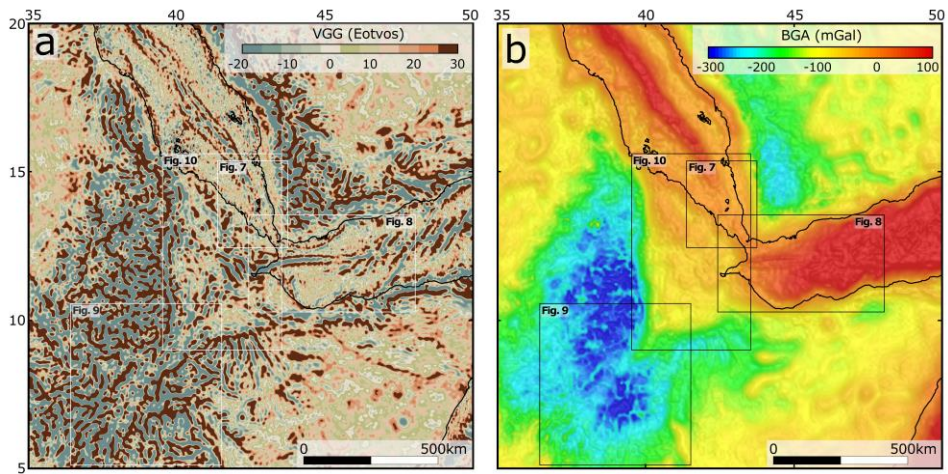


982 Fig. 4.

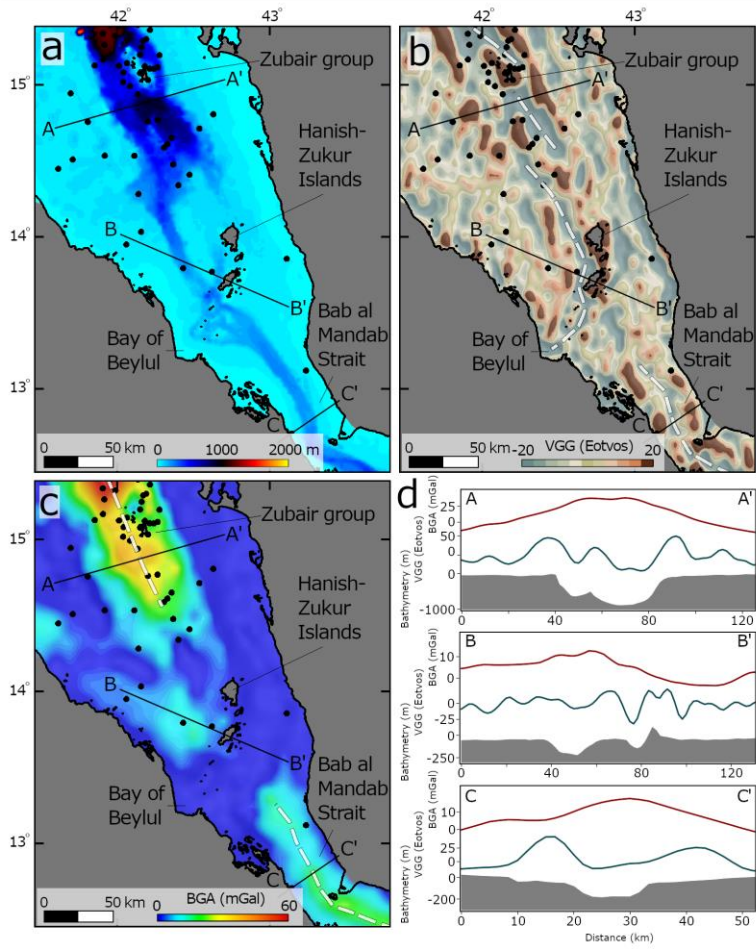


983

984 Fig. 5.

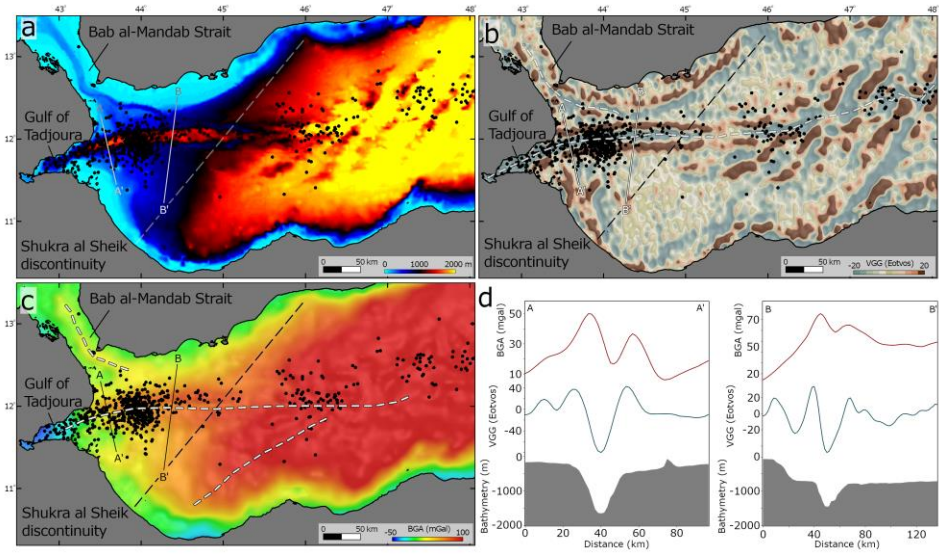


985
986 Fig. 6.



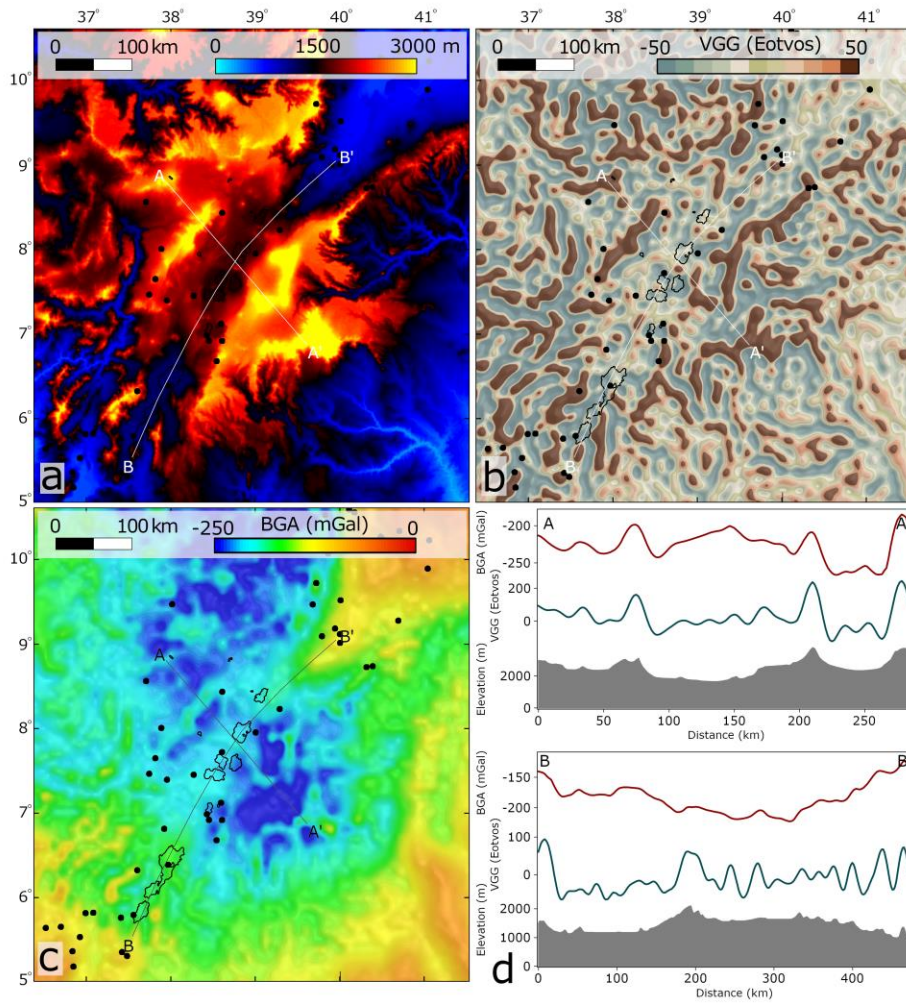
987

988 Fig. 7.

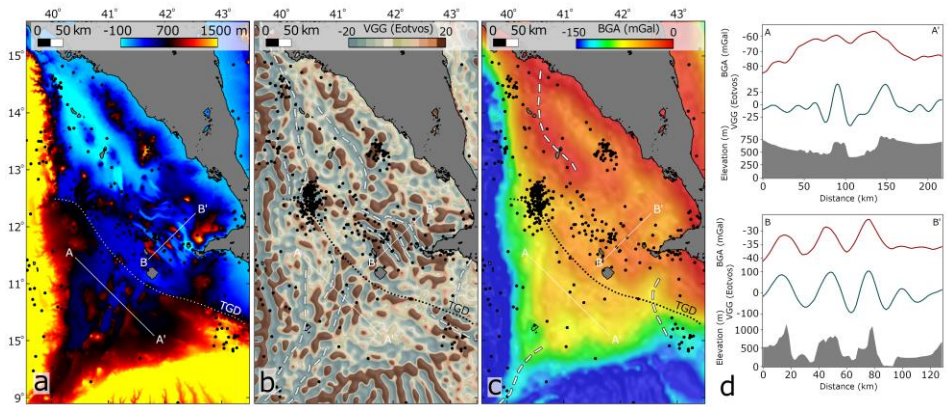


989

990 Fig. 8.

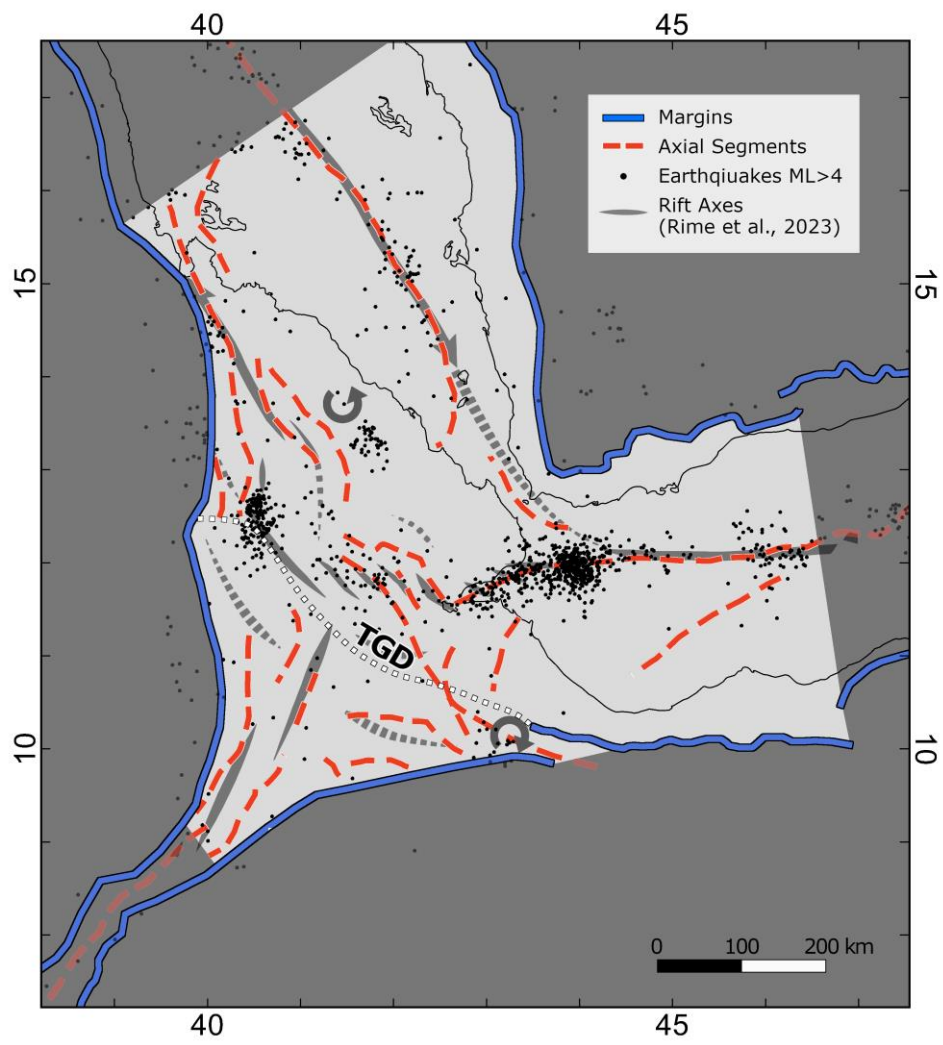


991
992 Fig. 9.

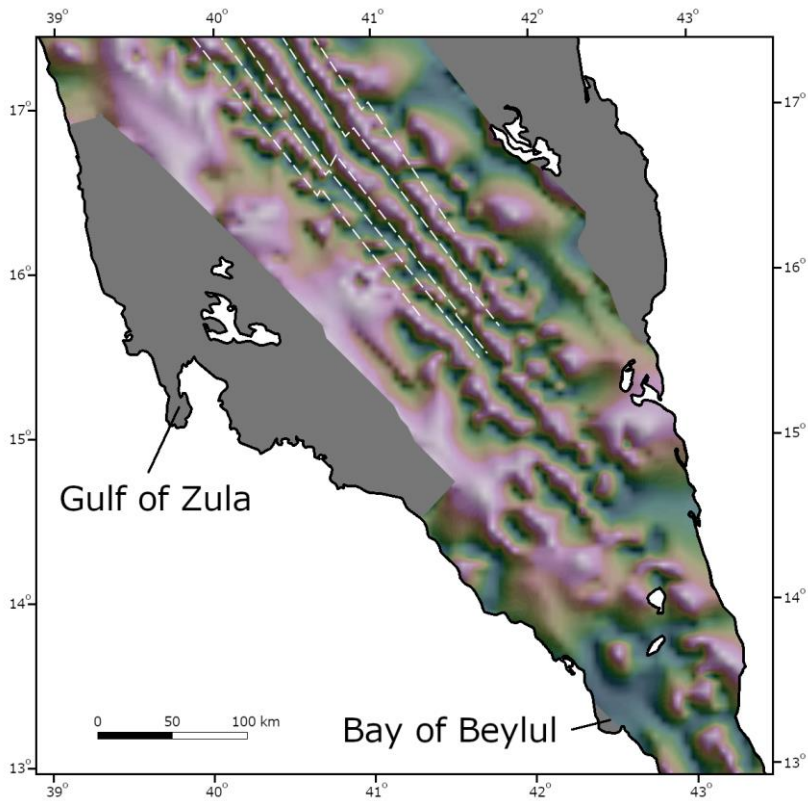


993

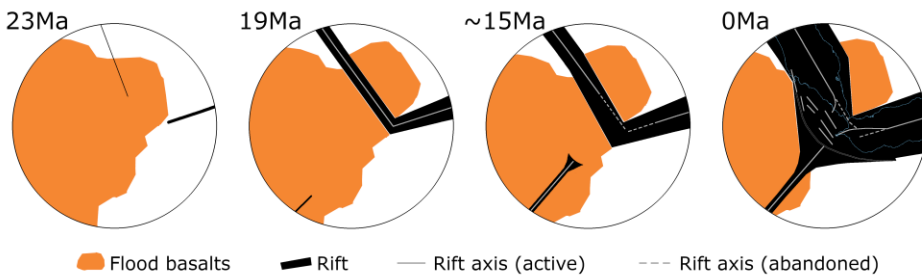
994 Fig. 10.



995
996 Fig. 11.



997
998 Fig. 12.



999
1000 Fig. 13.